

Prospects of Probing the Radio Emission of Lunar UHECRv Events

A. Aminaie^{a,*}, L. Chen^b, H. Pourshaghghi^{c,d}, S. Buitink^e, M. Klein-Wolt^c, L. V. E. Koopmans^f, H. Falcke^{c,g}

^aDepartment of Physics, University of Oxford, OX1 3RH, UK

^bNational Astronomical Observatories, Chinese Academy of Sciences, Beijing, China

^cDepartment of Astrophysics/IMAPP, Radboud University, Nijmegen, P.O. Box 9010, 6500 GL Nijmegen, The Netherlands

^dEindhoven University of Technology, PO Box 513, 5600 MB Eindhoven, The Netherlands

^eAstrophysical Institute, Vrije Universiteit Brussel, Pleinlaan 2, 1050 Brussels, Belgium

^fKapteyn Astronomical Institute, University of Groningen, PO Box 800, NL-9700 AV Groningen, The Netherlands

^gASTRON, Oude Hoogeveensedijk 4, 7991 PD Dwingeloo, The Netherlands

Abstract

Radio detection of Ultra High Energetic Cosmic Rays and Neutrinos (UHECRv) which hit the Moon has been investigated in recent years. In preparation for near-future lunar science missions, we discuss technical requirements for radio experiments onboard lunar orbiters or on a lunar lander. We also develop an analysis of UHECRv aperture by including UHECRv events occurring in the sub-layers of lunar regolith. It is verified that even using a single antenna onboard lunar orbiters or a few meters above the Moon's surface, dozens of lunar UHECRv events are detectable for one-year of observation at energy levels of 10^{18} eV to 10^{23} eV. Furthermore, it is shown that an antenna 3 meters above the Moon's surface could detect lower energy lunar UHECR events at the level of 10^{15} eV to 10^{18} eV which might not be detectable from lunar orbiters or ground-based observations.

Keywords: UHECRv, Cosmic Rays, Cosmic Neutrinos, Lunar Lander, Lunar Orbiter, Space Radio Experiment

1. Introduction

Radio emission from the cascades of energetic particles has been studied intensively in recent years. Particle accelerators such as Stanford Linear Accelerator Center (SLAC) produces radio emission from particle cascades (Saltzberg et al., 2001), (Belov et al., 2015). Along with lab experiments, radio experiments for studying the cosmic energetic particles in air showers and on the lunar surface are being developed. These experiments help to investigate the fundamental questions about the UHECRv such as their origin and the acceleration mechanism. The Moon has been long known as a detector for UHECRv events. The unique properties of Moon regolith such as very low conductivity and low attenuation makes it an ideal environment for detection of coherent radiation based on

the Askaryan Effect (Askaryan, 1965). We refer to this radio emission, also known as Cherenkov-like radiation, as Askaryan radiation through the paper (as stated in (James et al., 2011) and (ter Veen et al., 2010)). Askaryan radiation is spread over a broad spectrum covering microwave frequencies (GHz band corresponds to cm wavelengths) in dielectric solids, but it may also reach a peak at lower frequencies within tens of MHz (Scholten, 2007). Most of radio UHECRv experiments at MHz regime operate, however, at frequencies higher than 100 MHz where dispersion in the Earth's ionosphere, and the Galactic background noise, become low. Also the dimension of antennas becomes reasonably smaller at higher frequencies. In our analysis frequencies of 1.5 GHz and 150 MHz represent the GHz and MHz frequency regimes. From theoretical estimates (Zas et al., 1992) and the SLAC experiments (Saltzberg et al., 2001) can be understood that the dominant mechanism for producing lunar UHECRv radiation is charge excess. This is mainly

*Corresponding author

Email address: amin.aminaei@physics.ox.ac.uk (A. Aminaie)

due to the absence of strong magnetic fields, such as the Earth’s magnetic field, which is a key element in radio emission of air showers. The impact of energetic charged particles with lunar regolith generates electromagnetic pulses which develop and propagate as a cascade of electric currents through the layers of lunar regolith and lunar exosphere. Antennas onboard lunar orbiters, a lunar lander or a ground-based array can detect these events by measuring corresponding electric fields (also known as the lunar Askaryan technique (Dagkesamanskii and Zheleznykh, 1989)). In this paper we generalize the analytical methods in the literature for calculating the UHECRv apertures of ground based arrays so it can be used also for lunar orbiter experiments as well as for antennas on the Moon’s surface. For the latter we modified the method and included the events occurring in the sub-layers of lunar regolith. The results are used to estimate the number of events that can be detected for various radio experiments for a one-year observation.

- Radio Experiments of Lunar UHECRv Emission
- Analysis of Lunar UHECRv Events
- Categorization of Lunar UHECRv Events
- Technical Requirements of Future Lunar Radio Experiments
- Summary and Conclusion

2. Radio Experiments of Lunar UHECRv Emission

Radio detection of lunar UHECRv emission is limited by antenna sensitivity which depends on the effective collecting area of antennas. Thus large ground-based antenna arrays provide the highest sensitivity, however, the measured electric field of lunar UHECRv emission is weak because of the distance. Another limiting factor is the physical area of the Moon which is illuminated by antennas. As shown in Fig.1, the physical area depends on the beamwidth of the antenna and its distance from the lunar surface. The larger the area the higher chance of detection of lunar UHECRv events. A probability function then relates the physical area to the actual aperture for detection of UHECRv events. The probability function depends on the electromagnetic properties of UHECRv. It also depends

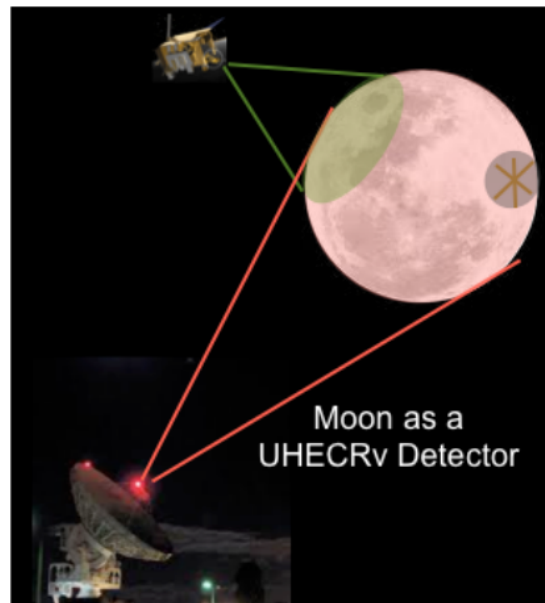


Figure 1: Observations of lunar UHECRv events using ground-based, lunar orbiter and Moon’s surface radio experiments. Dimensions are not to scale.

on system parameters that we will shortly present. There are various experiments capable of detection of Lunar UHECRv events (Bray, 2016). We compare the expected outcome of the Low Frequency ARray (LOFAR) (Horandel et al., 2009) and the Square Kilometer Array (SKA) (Bray et al., 2014) telescopes with observations from a lunar orbiter or the lunar surface (e.g. antenna onboard a lunar lander).

2.1. Lunar UHECRv Experiments

Orbital Low Frequency ARray (OLFAR) (Bentum et al., 2009) and Lunar Orbiter Radio Detector (LORD) (Gusev et al., 2006), (Raybov et al., 2016) are examples of planned Lunar Orbiter Observations of UHECRv events. We analyze the UHECRv detections from different altitudes and compare the expected results with results of simulations of UHECRv events from a tripole antenna at 100 MHz onboard lunar orbiter satellites (Stål, 2007). For observations of UHECRv events on the lunar surface, the analysis is done for an individual antenna onboard a lunar lander. It is based on the preliminary analysis (Aminaei et al., 2013) of the Lunar Radio eXplorer (LRX) experiment. LRX is a dedicated radio experiment initially designed for the proposed European lunar lander mission. LRX

includes a tripole antenna and a sensitive digital receiver in the frequency range of 5kHz-100MHz. The experiment was designed to observe radio emissions on the lunar surface including UHECRv radiation. Technical requirements and science cases of LRX are described in (Klein-Wolt et al., 2012; Zarka et al., 2012).

An individual antenna is used for both the lunar orbiter and the lunar surface experiments in this study. The analysis can be extended for multiple lunar orbiter antennas or for an array of antennas on the Moon's surface.

For all observations, UHECRv events can be detected if the maximum electric field of Askaryan radiation is equal to or greater than the minimum electric field detectable by the receiver. For Askaryan radiation, we use the formula presented in (James and Protheroe, 2009) and (Gayley et al., 2009). Furthermore, we extend the analysis by applying formulas in (James and Protheroe, 2009) for both the lunar regolith and sub-regolith. Based on these formulas, the electric field caused by Askaryan radiation depends on the energy of particles, the distance from the observer and frequency of observation. The minimum detectable electric field is defined (Gorham et al., 2004) by characteristics of the antenna and receiver, and electromagnetic properties of the dielectric (e.g. lunar regolith and sub-regolith).

$$\epsilon_{\min} = N_{\sigma} \cdot (2k_b)^{1/2} \cdot \left(\frac{T_{\text{sys}}}{A_e \Delta v}\right)^{1/2} \cdot \left(\frac{Z_0}{n_r}\right)^{1/2} \quad (1)$$

The dependence of the minimum detectable electric field (ϵ_{\min} , V/m) on system parameters and lunar environment is shown in Eq.1. N_{σ} is the minimum number of standard deviations needed to reject statistical noise pulses and is set to 5 in our analysis and k_b is Boltzmann's constant. T_{sys} is system noise temperature, A_e is the effective collecting area of the antenna(s) and Δv is the bandwidth of the receiver. In the last term Z_0 and n_r represent characteristic impedance ($Z_0 = 377 \Omega$) and the refractive index of the lunar surface respectively. The radiation transmission occurs when the ray reaches the surface at an angle of incidence which is bigger than the complement of the Cherenkov angle ($\theta_c = \cos^{-1}(1/n_r)$). For plane waves, the transmission rate is defined with the transmission coefficient (t_{\parallel}) as follows: (Williams, 2004)

$$t_{\parallel} = (n_r \cdot \cos \beta / \cos \beta_0 \cdot (1 - r_{\parallel}^2))^{0.5} \quad (2)$$

Where β is the angle of incidence to the Moon's surface normal and β_0 is the angle of refraction relative to the normal (outside the Moon's surface) as the rays pass through the Moon's surface into free space or through the sub-regolith into the lunar regolith. r_{\parallel} is the field reflection coefficient and the polarisation is assumed to be in the plane of incidence. A further numerical technique has been developed in (Williams, 2004) to convert this plane-wave transmission coefficient to the coefficient which meets the criteria for UHECRv rays within the observed solid angle.

A constant approximation of $t_{\parallel} = 0.6$ has been used in (Gayley et al., 2009) which we also used for our analysis.

2.2. Frequency of UHECRv Observation

UHECRv radio emission covers a broad frequency range from kHz to GHz regime. Ground based radio experiments of UHECRv are common in MHz bands. LOFAR, SKA Low and Westerbork Synthesis Radio Telescope (WSRT lower band, NuMoon (Scholten et al., 2009)) are examples of MHz radio telescopes for detection of lunar UHECRv events. SKA Mid2, the higher band of the WSRT array, the Goldstone Lunar Ultra-high-energy Neutrino Experiment (GLUE, (Gorham et al., 2004)), the Lunar Ultra-high-energy Neutrino Astrophysics with the Square Kilometre Array (LUNASKA, (James et al., 2010)), the Radio EVLA Search for Ultra-high-energy Neutrinos (RESUN, (Jaeger et al., 2010)) and Five-Hundred-Meter Aperture Spherical Radio Telescope (FAST) (Nan et al., 2011) are examples of GHz experiments for UHECRv events. A series of past and near-future lunar radio experiments for detection of UHECRv events are described in (Bray, 2016).

In this study, we analyse the UHECRv events with the energy of 10^{15} eV to 10^{23} eV. This energy level is in accordance with the discovery of the PeV neutrinos by IceCube (Aartsen et al., 2013a), (Aartsen et al., 2014), where the possibility of the existence of neutrinos with energy above 100 PeV is now being considered. The corresponding physics including the cross-section of this regime of neutrinos are discussed in the literature. (e.g. (Marfatia, McKay and Weiler, 2015))

We use frequencies of 150 MHz and 1.5 GHz as indicators of UHECRv observations in MHz and GHz bands. These are the same frequencies used in the reference papers (Gayley et al., 2009) and (Jeong et al., 2012).

Lunar UHECRv events at low frequencies also have been investigated using numerical methods (Stål, 2007), (Gusev et al., 2006).

In our analysis, the bandwidth (B.W.) is roughly set to 13% of central frequency (f_c) (20 MHz for f_c of 150 MHz and 200 MHz for f_c of 1.5 GHz). The antenna in this analysis is assumed to be a simple resonance antenna, which is optimised at its central frequency. Thus only a narrow bandwidth would allow for a widebeam and omnidirectional radiation pattern in this design. Using this antenna at a broader bandwidth requires additional components for impedance matching. Also at a broader frequency range, side-lobes appear in the radiation pattern, which makes the calibration complicated. Coherent Askaryan radiation is the dominant radio emission generated by the UHECRv events at both frequency regimes. For a lunar lander antenna, surface waves are the main mechanism for propagation of the radiation of those events which occur at a far distance on the Moon's surface. At low frequencies, kHz up to a few MHz, transition radiation might be also important as the emission mechanism (Sinha and Datta, 2012) for upcoming neutrinos interacting very near the lunar surface.

The selected frequency band at 150 MHz is within the optimum frequency window where the wavelength is of the order of the length of the shower. As a result, it produces a more isotropic UHECRv radio emission (Scholten, 2007).

2.3. Antenna and Receiver

A tripole antenna is a preferred choice for individual antennas onboard the lunar orbiter satellites and lunar lander (Stål, 2007; Klein-Wolt et al., 2012). It consists of 3 co-centred orthogonal dipoles which enables it to detect signals in all directions. In principle, a single tripole antenna is capable of localising radio emissions with a few degrees resolution (Chen et al., 2010). Considering half-wavelength (resonance) dipoles as the optimal design, the length of dipoles would be around 1 m for f_c of 150 MHz and 10 cm for f_c of 1.5 GHz which make them suitable for space-based experiments. In contrast, the large size of antenna at kHz frequencies could be an issue for lunar missions. The exact length and orientation of antenna should be optimised based on the lunar environment and system characteristics.

In our analysis for onboard antennas, the gain of the antenna is set to 1 so antennas are assumed to be omnidirectional. The corresponding A_e in

Eq.1 then becomes $A_e = \lambda^2/4\pi$ where λ is the wavelength of the operational frequency. This assumption simplifies the calculation of Eq.1 otherwise A_e becomes a complicated function of the antenna gain and should be calculated for each frequency over the entire bandwidth.

The receiver sensitivity is identified with the minimum detectable electric field. We apply the formula (Eq.1) presented in (Gorham et al., 2004) and (Gayley et al., 2009). For the 150 MHz band, the dominant system noise in the selected B.W. is Galactic noise and it varies between 820° K (for 100 MHz) and 142° K (for 200 MHz) (Oberoi and Pinçon, 2005). In the meantime, the Moon's noise temperature varies in a wide range from 130° K to 400° K (Pugacheva and Shevchenko, 2000) which also means that only Extreme Temperature Electronics (ETE) can be operational on the Moon's surface. By using a Low Noise Amplifier (LNA) which typically has a noise figure below 1.5 (equivalent to noise temperature lower than 120° K) at the first input of the receiver, the dominant noise is usually Galactic noise at MHz regime. In our analysis, the Galactic noise temperature at central frequency (294° K, 150 MHz) has been used as the system noise. This is roughly equal to the noise temperature of a receiver with a noise figure of 3 dB. With noise temperature of 294° K, the minimum detectable electric field for the receiver becomes $2.63 \mu\text{V}/\text{m}$ per MHz which can be improved by using more antennas. For 1.5 GHz the dominant noise temperature is generated by electronics and depends on system design and operating environment. For our analysis at 1.5 GHz we used a conservative receiver temperature of 300° K, roughly the same as amount of the dominant noise at 150 MHz. The corresponding minimum detectable electric field for a receiver at 1.5 GHz becomes $8.41 \mu\text{V}/\text{m}$ per MHz, which is more than three times at 150 MHz. Therefore only UHECRv events at higher radiation amplitude are expected to be detected at 1.5 GHz. As we will see this is reflected in the event rate predictions of the two frequency regimes. For ground-based observation, minimum detectable electric field is set at $0.01 \mu\text{V}/\text{m}$ per MHz, a typical number which has been used in (Gayley et al., 2009) and (Jeong et al., 2012). For simplicity, we assume the bandwidth and T_{sys} of such an array to be the same as those for a lunar lander or lunar orbiter antenna. ($T_{\text{sys}}=294^\circ$ K and B.W.=20 MHz for 150 MHz, $T_{\text{sys}}=300^\circ$ K and B.W.=200 MHz for

1.5 GHz). This gives the collecting area of the array as 22100 square meters for 150 MHz and 2255 square meters for 1.5 GHz. It should be noted that the same sensitivity can be achieved with a smaller collecting areas if a broader B.W. is used. For instance, by using the B.W. of 100 MHz at a central frequency of 150 MHz, the collecting area can be reduced to 4420 square meters. For a frequency of 1.5 GHz and B.W. of 0.5 GHz, the collecting area of 902 square meters would be needed to reach the sensitivity of $0.01 \mu\text{V}/\text{m}$ per MHz. In tables 1 and 2, a summary of receiver parameters in GHz and MHz used in this study is shown. In the next section the analysis method and results for UHECRv events are discussed.

3. Analysis of Lunar UHECRv Events

3.1. Lunar Cosmic Ray Events

We use the method developed in (Jeong et al., 2012) for detection of UHE Cosmic Rays colliding with the Moon. Cosmic Rays, containing energetic primary particles, unlike neutrinos, can not penetrate through the lunar regolith, therefore, CR events only occur on the lunar surface. The radio emission then propagates mostly through the lunar exosphere where radio wave attenuation can be neglected. The calculation is based on UHECR aperture which is the physical aperture illuminated by the antenna times a probability function. Here we show it as $P_{CR}(E)$ and it is the probability of CR interaction with the Moon's surface which produces Askaryan radiation in the aperture. $P_{CR}(E)$ depends on the frequency of observation, Askaryan radiation characteristics and lunar environment properties including refractive index. It also includes the contribution from smooth surface and surface roughness. The formula for UHECR aperture is presented in (Jeong et al., 2012) and we use it for different experiments as follows. For the lunar lander, the antenna is assumed to be 3 m above the lunar surface which was the height of the ESA lunar lander planned for LRX. For lunar orbiters, results for an individual antenna at altitudes of 100, 500 and 1000 km from the lunar surface are shown. Also, results for ground-based arrays are shown for two frequency regimes. We use the same sensitivity taken from Eq.1 for individual antennas but the field of view (FoV), and as a result the area of the

Moon's surface covered by a lunar lander antenna or the lunar orbiter antennas, depends on the distance of antenna from the Moon's surface. In the next section the corresponding aperture for each case is calculated.

3.1.1. Aperture, Flux Density and Event Rate of UHECR Events

UHECR Apertures at 1.5 GHz vs. energy are illustrated in the top plot of Fig.2. For all results the apertures are a small portion of the actual aperture of Moon's surface illuminated by antenna:

$$Ap = A_0 \cdot P_{CR}(E)(\text{km}^2 \cdot \text{Sr}), A_0 = 2\pi \cdot \pi R_0^2(\text{km}^2 \cdot \text{Sr}) \quad (3)$$

Where R_0 is the radius of lunar surface which is covered by antenna radiation pattern. An omnidirectional pattern is assumed for antennas on the Moon's surface. For lunar orbiter and ground based antennas, it is assumed that the surface is illuminated with the antenna main-lobe so the gain is constant over the whole beamwidth. Under these conditions R_0 depends on the distance of antenna from the lunar surface and can be calculated using simple geometry. Maximum R_0 , R_{ap} , for various distances are included in table 3. Detectable UHECR events can occur within a radius of R_0 from the point where antenna is vertically mapped to the lunar surface. Therefore the total aperture is integrated over $A_0(r) \cdot P_{CR}(E, r)$ where r varies between 0 and R_{ap} . (See Appendix A)

Although physical aperture increases at larger distances, Askaryan radiation at the position of the antenna becomes weaker due to the distance. As a result, the detection of UHECR events is a compromise between the distance of antenna and size of aperture. This has been reflected in simulated results in Fig.2. The apertures are shown via energy of cosmic rays in a broad range from 10^{18} eV to 10^{23} eV. The possibility of the detection of UHECRv events increases with the primary energy of events, however the detectable aperture is limited by the physical aperture of the Moon's surface which is illuminated by the antenna. This is particularly the case for antenna at 3 m height whose aperture is almost constant over a broad range of energy (Fig.2 and Fig.3). As distance increases, lower energy events become undetectable but the size of aperture increases significantly. At energies of 3×10^{20} eV and higher the aperture reaches a threshold as the radius of aperture becomes comparable to the lunar radius. Therefore antenna on

Radio Observation	f_{min}	f_{max}	$B.W.$	f_0	$E_{min}(V/m/MHz)$	Frequency Band
Lunar Lander	1.4	1.6	0.2	1.5	8.41×10^{-6}	GHz
Lunar Orbiters	1.4	1.6	0.2	1.5	8.41×10^{-6}	GHz
Ground-based array	1.4	1.6	0.2	1.5	1×10^{-8}	GHz
SKA1 MID2	0.950	1.760	0.81	1.355	2.1×10^{-9}	GHz

Table 1: Receiver parameters of radio UHECRv observations in GHz band. Frequencies and bandwidths are in GHz.

Radio Observation	f_{min}	f_{max}	$B.W.$	f_0	$E_{min}(V/m/MHz)$	Frequency Band
Lunar Lander	140	160	20	150	2.63×10^{-6}	MHz
Lunar Orbiters	140	160	20	150	2.63×10^{-6}	MHz
Ground-based array	140	160	20	150	1×10^{-8}	MHz
SKA1 LOW	50	350	300	200	1.4×10^{-9}	MHz
LOFAR	110	130	20	120	6.62×10^{-9}	MHz

Table 2: Receiver parameters of radio UHECRv observations in MHz band. Frequencies and bandwidths are in MHz. E_{min} LOFAR is calculated from the array parameters in Scholten (2007).

Distance from Moon	$R_{ap}(km)$	which makes it an optimum distance for radio observations of lunar UHECR events at 150 MHz.
Lunar Lander: 3 m	3.23	In the bottom plot of Fig.3, corresponding flux limits of various experiments are shown and simulated results are compared with the expected outcome for 30 days of UHECR observation with LOFAR.
Lunar Orbiters: 100 km	565.46	In both frequency regimes, the events with energy lower than 10^{19} eV can only be detected by antenna on the Moon's surface.
500 km	1095	Using calculated apertures and standard flux densities of UHECR, it is possible to estimate the event rate of each experiment. Here we use predicted flux for the occurrence of UHECR presented in (Abraham et al., 2010). The model and expected event rates for various lunar observations are shown in Fig.4. The model is for UHECR with energy level between 10^{17} and 10^{21} eV. At this range of energy of UHECR and using calculated apertures, expected detectable event rate are calculated. The results are shown for two frequency regimes (1.5 GHz in blue and 150 MHz in red) for a 1-year observation. By comparing the number of expected events per year, it can be seen that no UHECR events using Earth-based observation with ($E_{min} = 0.01\mu V/m/MHz$) within this window of energy would be detected. Also from the UHECR flux in Fig.4 one would expect that most of the expected events has an energy in the range of 10^{17} to 10^{18} eV where the flux density is high. The lunar lander antenna becomes particularly important for detection of lunar cosmic ray events at lower energy range where other experiments can not detect these events due to the weak signal. We will discuss this in details in 4.1.
1000 km	1343	
Ground-based array: 380000 km	1738 (Moon's Rad.)	

Table 3: Radius (R_{ap}) of physical area on the Moon's surface in the field of view of omnidirectional antennas at various distances from Moon.

lunar orbiters at order of 500 km -1000 km would be the optimum distance for detecting lunar UHECR events. In Fig.2 apertures of ground-based observation and SKA Mid2 (190 SKA antennas) are also shown for comparison. In the bottom plot, the corresponding flux limits of the above experiments are shown. The illustrated flux results ($E_{cr}^2 \Phi_{cr}$) represent the detectable flux densities of UHECR events for a 1-year observation for 90% confidence limits (e.g. (Stål, 2007)).

The same method has been used to extract apertures for UHECR events at 150 MHz. Results are illustrated in Fig.3. Comparing with Fig.2, it can be seen that aperture at higher energy levels is proportional to the square of wavelength. ($A_p \propto \lambda^2$). The curves of detectable CR events are slightly shifted towards the lower energy levels at GHz band. For instance, this is seen for the aperture of a ground-based array with the same sensitivity where at 150 MHz the detectable events begin around 6×10^{20} eV compared with 10^{20} eV for 1.5 GHz. Similar to the apertures at 1.5 GHz, there are small changes in the size of the aperture at distances higher than 500 km

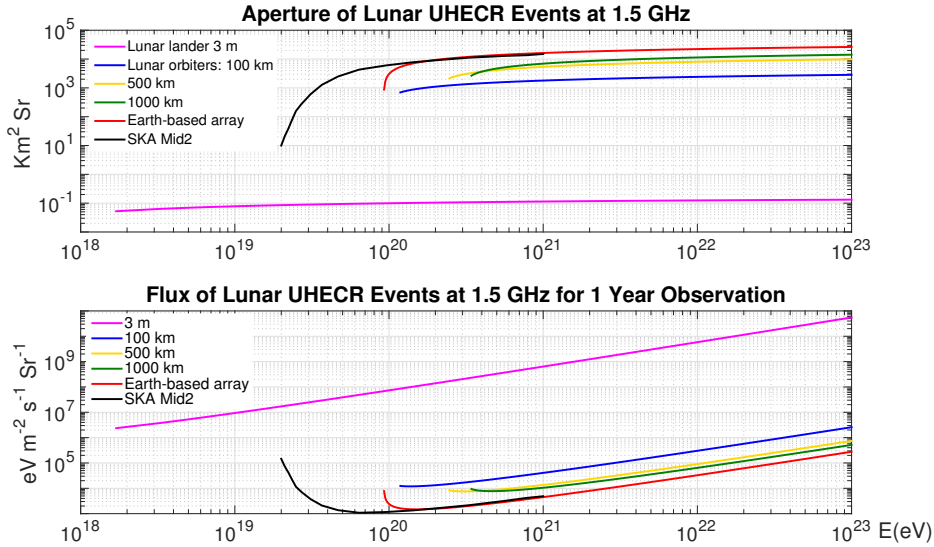


Figure 2: Top, Apertures of UHE Cosmic Rays for individual antenna onboard a lunar lander 3 m above Moon’s surface and onboard lunar orbiters at altitudes of 100 km, 500 km, 1000 km with a sensitivity of $8.41 \mu\text{V}/\text{m}/\text{MHz}$, also for ground-based array with the sensitivity of $0.01 \mu\text{V}/\text{m}/\text{MHz}$. Results are compared with the aperture of SKA Mid2 (reproduced from (Bray et al., 2014)). See table 1 for receiver parameters. Bottom, corresponding flux limits of UHE Cosmic Rays for a 1-year observation at 1.5 GHz.

3.2. Lunar Cosmic Neutrino Events

We modified method in (Gayley et al., 2009) to analyse lunar neutrino events (UHECv) for various experiments. Here are the main assumptions:

$$- E_s = 0.2.E$$

For neutrino events only 20% of energy of neutrinos is converted to the hadronic shower while $E_s = E$ for Cosmic Rays (e.g.(Bray, 2016)).

Similar to Cosmic Rays, an aperture is defined based on the physical aperture covered by antenna radiation pattern and a possibility of the occurrence of UHECv events:

$$Ap = A_0 \cdot P_v(E)(km^2.Sr), A_0 = 4\pi \cdot \pi R_0^2(km^2.Sr) \quad (4)$$

While for UHECR only downward CR are taking into account, both upward and quasi-horizontal downward neutrinos are effective so a full sphere (4π) solid angle is applied for calculation of UHECv apertures. Similar to cosmic rays, contribution from surface roughness is included in $P_v(E)$ as it scatters the radiation for surface events. Results of analysis show that at selected frequencies the major contribution is from downward neutrinos. This is consistent with results of ground-based observations in (Gayley et al., 2009). More recent stud-

ies suggest that small-scale surface roughness could have greater contribution in some UHECrv events but on average, the contribution of surface roughness would be small (James, 2013).

For an antenna 3 m above the lunar surface, we add the possibility of UHEv events occurring in the lunar sub-regolith. This is done using the formula presented in (James and Protheroe, 2009) and by taking into account the attenuation of radio wave propagation through the lunar regolith. Typical numbers for refractive index of lunar regolith ($n_r=1.73$) and sub-regolith ($n_r=2.5$) (James and Protheroe, 2009), (Olhoeft and Strangway, 1975) have been used in the aperture calculation. This corresponds to dielectric constant (ϵ_r) of 3 and 6.25 respectively. For attenuation, the loss tangent of 0.01 ($\tan(\delta) = 0.01$) (Carrier et al., 1991) is set and the depth of regolith is assumed to be 10 m (Shoemaker and Morris, 1969). We chose loss tangent and depth of regolith as extreme cases to estimate the maximum attenuation of Askaryan radiation when passing through the lunar regolith. The attenuation reduces the maximum electric field of Askaryan radiation of sub-regolith. The sub-regolith aperture is calculated similar to the regolith aperture but the roughness effect has been

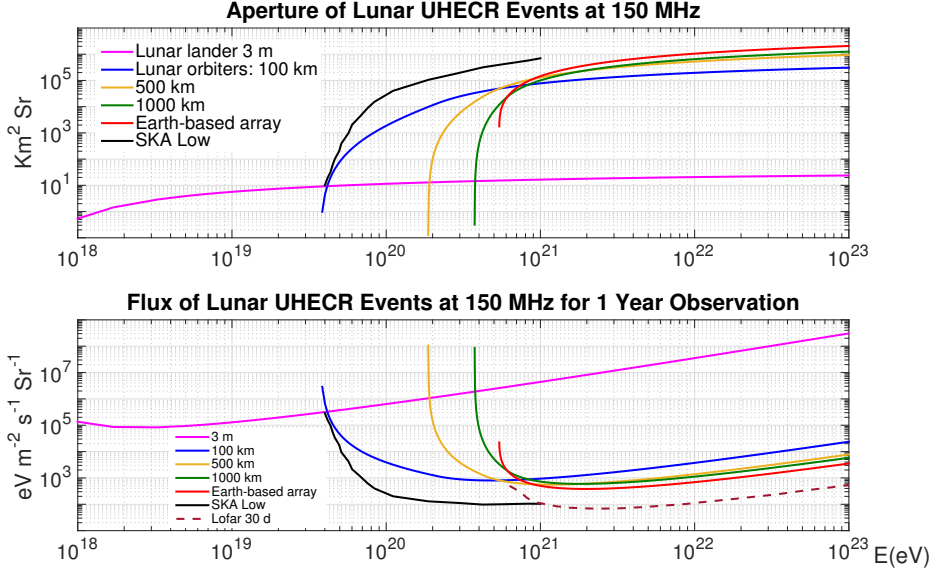


Figure 3: Top, Apertures of UHE Cosmic Rays for individual antenna onboard a lunar lander 3 m above Moon’s surface and onboard lunar orbiters at altitudes of 100 km, 500 km, 1000 km with a sensitivity of $2.63 \mu\text{V}/\text{m}/\text{MHz}$, also for ground-based array with a sensitivity of $0.01 \mu\text{V}/\text{m}/\text{MHz}$. Results are compared with the aperture of SKA Low (reproduced from (Bray et al., 2014)). See table 2 for receiver parameters. Bottom, corresponding flux limits of UHE Cosmic Rays for a 1-year observation at 150 MHz. Results are compared with flux limit of LOFAR for a 30-day observation (reproduced from (Scholten, 2007)).

eliminated. This is because that sub-regolith radiation could face multiple internal reflections before reaching the surface therefore the effect of roughness over the whole aperture becomes complicated. The calculation for sub-regolith, therefore, represent lower limits to the apertures but as discussed, the roughness effect has a small contribution in calculation of the apertures. The total aperture for UHEC neutrinos then becomes a virtual sphere which covers both events on the lunar surface and those which occur inside the lunar regolith. The details of calculation are explained in Appendix A. In this analysis only the attenuation of the direct path between lunar sub-regolith and antenna is taken into account. However, the radiation generated in a cascade shower could in principle face multiple reflections through sublayers and the antenna might receive a superposition of radio emission in various directions. This could be particularly significant for distant lunar observations where contributions from multiple cascades of Askaryan showers result in a global radiation, which would be different from individual local radio emission. This is the case for the effect of sub-layers of the Moon regolith for both lunar orbiter and ground based experiments. The analysis requires further investigations and we

leave it for future study.

3.2.1. Aperture, Flux Density and Event Rate of UHECv Events

Apertures of lunar UHECv events at 1.5 GHz for various distances are shown in Fig.5. Compared with UHECR apertures at the same frequency, UHECv apertures have been roughly decreased by the order of 100, but it follows a similar trend. For an antenna 3 m above the lunar surface and sensitivity of $8.41 \mu\text{V}/\text{m}/\text{MHz}$, aperture covers the entire range of energy from 10^{19}eV to 10^{23}eV . As opposed to CR aperture, the aperture increases almost linearly from about $0.001 \text{ km}^2\text{Sr}$ at the energy of 10^{19}eV to $10^{-1} \text{ km}^2\text{Sr}$ at the energy of 10^{23}eV . For 100 km distance, detectable events begin at $6 \times 10^{20}\text{eV}$. As the orbiter distance increases, only energetic UHECv events at higher levels become detectable so that for 1000 km the detectable events begin around $2 \times 10^{21}\text{eV}$. For Earth-based arrays with a sensitivity of $0.01 \mu\text{V}/\text{m}/\text{MHz}$, detection of UHECv events begins at energy of $5 \times 10^{20}\text{eV}$. Similar to UHECR apertures, lunar orbiter experiments at 500 km and 1000 km distance approach a constant level at the highest energy level. As a result, it seems that this range

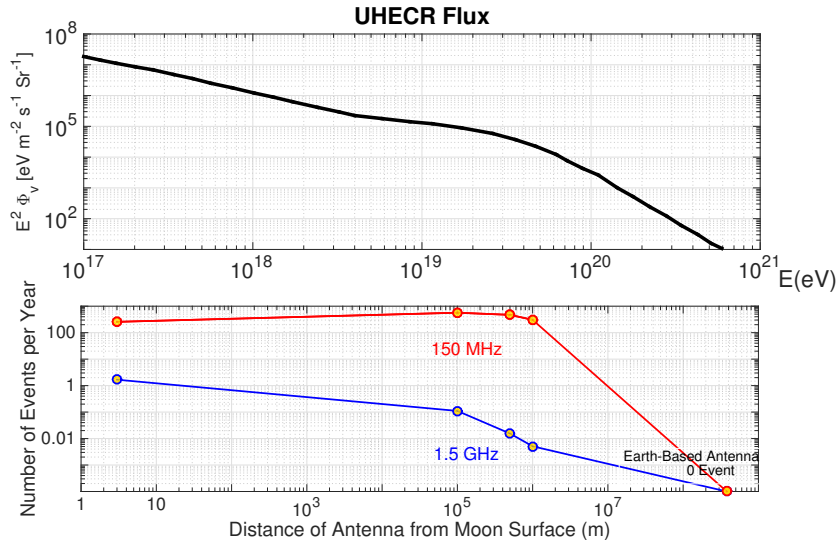


Figure 4: Top, predicted UHECR flux model (reproduced from (Abraham et al., 2010)). Bottom, prediction of number of events for 1-year observations of UHE Cosmic Rays for antennas onboard a lunar lander 3 m above the Moon’s surface and onboard lunar orbiter satellites at altitudes of 100 km, 500 km, 1000 km and Earth-based antenna array (all marked with yellow circles). Results are shown for both frequencies of 150 MHz (Red) and 1.5 GHz (Blue).

of altitudes is an optimum distance for lunar observations of UHECR ν events. In the bottom plot of Fig.5, corresponding flux limits of UHECR ν apertures for a 1-year observation are plotted. For comparison, the flux limit of SKA Mid2 (see table 1) for 1000 hours of observations is also plotted (Bray et al., 2014). Similarly, aperture and fluxes of lunar UHECR ν events at 150 MHz vs. distance are shown in Fig.6. Similar to CR, neutrino apertures are proportional to the square of wavelength at higher energy levels ($A_p \propto \lambda^2$). The minimum energy level of detectable neutrino events are also slightly shifted as the frequency changes. For instance, UHECR ν events at 100 km become detectable at 10²¹eV at 150 MHz compared with 5×10^{20} eV at 1.5 GHz (the receiver parameters are available in Tab.1, Tab.2). For Earth-based array, this is also the case where UHECR ν events can be observed from 3×10^{21} eV at 150 MHz and 4×10^{20} eV at 1.5 GHz (with array sensitivity of 0.01 μ V/m/MHz). The maximum aperture at highest energy levels approaches a constant level for altitudes of 500 km and 1000 km. The aperture of SKA Low is illustrated (Bray et al., 2014) in the plot for comparison. In the bottom plot of Fig.6, corresponding flux limits of UHECR ν events at 150 MHz for a 1-year observation are plotted. Flux limits of LOFAR (30 days) (Scholten, 2007) and SKA Low (1000 hours) (Bray et al., 2014) observation are shown in the

plot. It should be noted that data for SKA array only covers the antennas at phase I. For instance, the SKA2 MID2 will use 1,500 SKA antenna dishes (Bray et al., 2014). Also the flux limit for an individual antenna at 100 MHz for 1-year observation at 100 km and 1000 km on a lunar orbiter is shown (Stål, 2007). The results of (Stål, 2007) have been calculated using a numerical Monte Carlo method and the antenna parameters are different. As is expected, however, the aperture increases with the wavelength, and as a result the flux of UHECR ν events at 150 MHz approaches a lower limit compared with the one for 100 MHz.

Similar to (Stål, 2007), the expected lunar UHECR ν event rate for 3 models of neutrino process is presented in Fig.7. Neutrino flux models are reproduced on the top plot. The Greisen-Zatsepin-Kuzmin (GZK) model predicts GZK neutrinos which have a limit of about 5×10^{19} eV. GZK neutrinos are generated during the UHECR interaction with Cosmic Microwave Background (CMB) via the secondary pion decay process. The detection of neutrinos at the GZK limit are important because it justifies the observations of UHECR with energies above the GZK limit (Engel et al., 2001). Topological Defects (TD) (e.g. (Bhattacharjee et al., 1992)) and Z-Burst processes (e.g. (Weiler, 2003)) are the suggested models for the existence of neutrinos with energies well beyond the GZK limit. The lim-

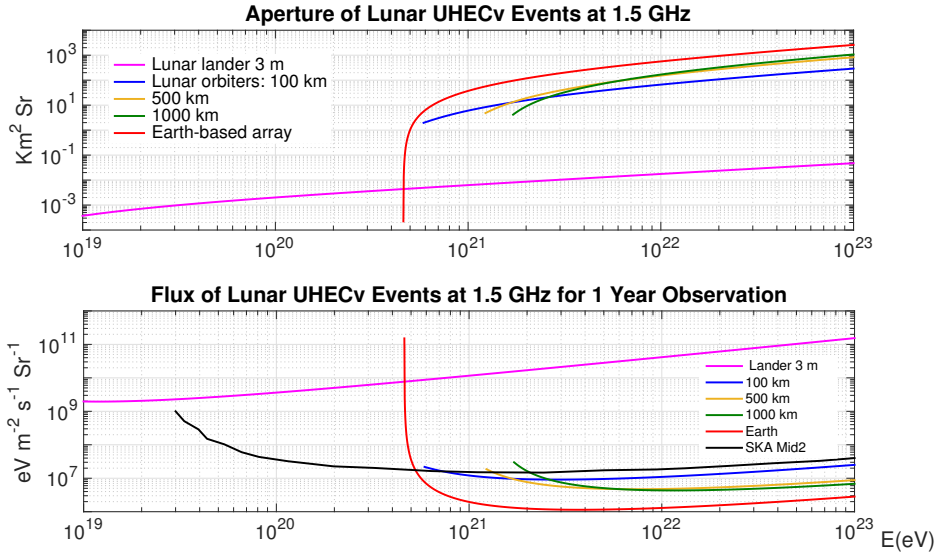


Figure 5: Top, Apertures of UHE Cosmic Neutrinos for individual antenna onboard a lunar lander 3 m above Moon’s surface and onboard lunar orbiters at altitudes of 100 km, 500 km, 1000 km with a sensitivity of $8.41 \mu\text{V}/\text{m}/\text{MHz}$, also for ground-based array with a sensitivity of $0.01 \mu\text{V}/\text{m}/\text{MHz}$. Bottom, corresponding flux limits of UHE Cosmic Neutrinos for a 1-year observation at 1.5 GHz. Results are compared with the aperture of SKA Mid2 for a 1000-hour observation (reproduced from (Bray et al., 2014)). (See table 1 for receiver parameters).

its of recent neutrino observations are illustrated in Fig.7. Z-Burst model, however, is ruled out by recent observations therefore for calculation of the occurrence of Z-Burst neutrinos, we apply the limit of ANITA-II (ANtarctic Impulse Transient Antenna) observations (Gorham et al., 2010). The ANITA-lite ν flux limit (Barwick et al., 2006) is well above the ANITA-II limit and is not shown in the figure. Also, the flux density models are not affected by the limits of IceCube (Aartsen et al., 2013a) and Auger (Aab et al., 2015) experiments. Based on the models, UHECv event rates are calculated for 1.5 GHz and 150 MHz observation. Results are illustrated vs. distance of antenna to the lunar surface. For 1-year observation at 1.5 GHz (bottom left), observations of GZK and TD neutrinos are unlikely for all experiments. Considering ANITA-II limit, Z-burst neutrinos (the most energetic events) are only expected to be detected by a lunar orbiter antenna and an Earth-based array.

For 1-year observations at 150 MHz (bottom right), detection of GZK neutrinos is not expected for all experiments. However, for an antenna 3 m above the lunar surface the event rate is 0.1. Thus an array of a hundred antennas on the lunar surface, for instance, would provide an ideal experiment for de-

tection of this interesting regime of neutrinos. TD neutrinos are only detectable for low distance experiments from the Moon (3 m, 100 km and 500 km). With applying the limit of ANITA-II observations to Z-Burst model, several hundred of lunar UHECv events are predicted for one-year observation of a lunar orbiter antenna or an Earth-based array. Overall, it seems that 150 MHz would provide a reliable window for radio observation of lunar UHECRv events. For Earth-based observations GHz band could be preferred as the effects of the Earth’s ionosphere such as dispersion becomes less important (Gorham et al., 1999). It should be noted that the distances from few meters above the Moon’s surface up to few tens of kilometer (which is the typical altitude of lunar orbiter satellites) are not realizable for lunar UHECRv experiments.

3.3. Validation of the Method

To examine the validity of the analysis, a comparison of the method used in this article has been made with the existing models to calculate the apertures of lunar UHECRv events for SKA-Low. Results are shown in Fig. 8 where curves on top (in blue) are the lunar UHECR apertures predicted for SKA-Low. The dashed curve in blue is taken

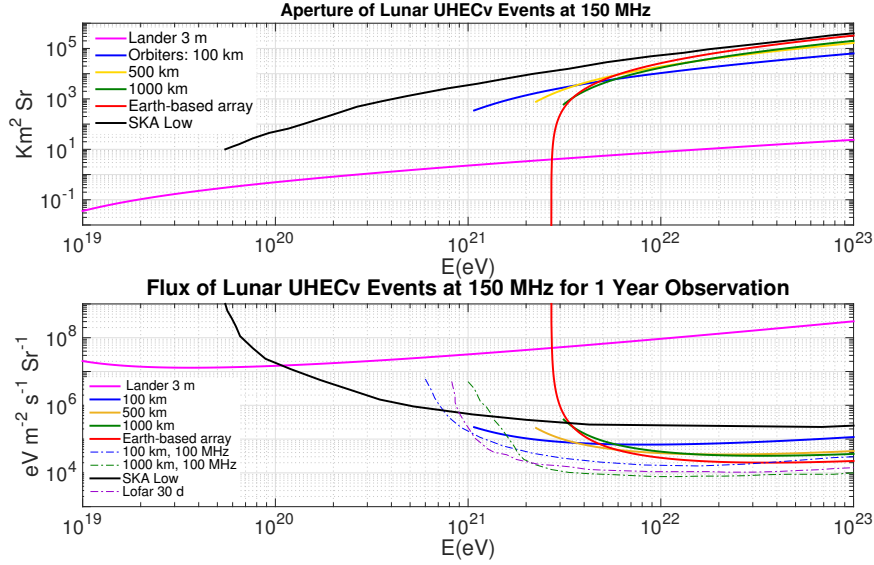


Figure 6: Top, Apertures of UHE Cosmic Neutrinos for individual antenna onboard a lunar lander 3 m above Moon’s surface and onboard lunar orbiters at altitudes of 100 km, 500 km, 1000 km with a sensitivity of $8.41 \mu\text{V}/\text{m}/\text{MHz}$, also for ground-based array with a sensitivity of $0.01 \mu\text{V}/\text{m}/\text{MHz}$ and SKA Low (Bray et al., 2014). Bottom, corresponding flux limits of UHE Cosmic Neutrinos for a 1-year observation at 150 MHz. Results are compared with aperture of SKA Low for a 1000-hour observation (reproduced from (Bray et al., 2014)), LOFAR, 30 days observation (Scholten, 2007), individual antenna at 100 MHz at 100 km and 1000 km lunar orbiter for 1 year observation (Stål, 2007). (See table 2 for receiver parameters)

from (Bray et al., 2014) which shows a max of 30% difference with the results of our simulation at 10^{20} eV. Between 10^{20} eV and 10^{21} eV the difference between the two curves decreases, and at 10^{21} eV two curves approach the same point at 8×10^5 km Sr. For energies higher than 10^{21} eV the data for the existing model was not available. The lower curves (in red) compare two models for detection of lunar neutrinos using SKA-Low parameters. It can be seen that the calculated lunar UHECv aperture is in good agreement with the existing model (Bray et al., 2014) between 3×10^{20} eV and 1×10^{23} eV. The difference is that the UHECv events are not detectable at energy levels lower than 3×10^{20} eV according to our analysis, while the energy limit for the existing model is 5×10^{19} eV. Possible explanation is that a full Monte Carlo simulation is used in (Bray et al., 2014) where includes differential cross-sections in which sometimes 100% of the neutrino energy would be converted to a hadronic cascade as opposed to 20% for our analysis. It also should be noted that the detectable aperture becomes very small and non-practical at the level of 5×10^{19} eV in our study.

3.3.1. The Angular Spread of the Observations

For all observations, a spherical symmetry is assumed so that the UHECRv events are detected randomly without specifying any preference over the viewing angle. In our analytical method, only the hadronic showers caused by a CR/ first interaction in the lunar regolith are considered. In principle, UHECRv events could also be detected by the second interactions. Examples are an upcoming UHECv event interacting in the regolith, with a secondary muon or tau. Also an initial neutral current interaction followed by a second interaction which could generate a secondary shower. Such a secondary shower is defined in the Monte Carlo simulation used in ANITA experiment (Mercurio, 2009). It, however, should be noted that the expected apertures only increase if the first UHECRv interaction is out of the antenna view. This scenario is ruled out in our analysis since in both lunar orbiter and lunar lander observations, the antenna is assumed to be an omnidirectional antenna with a wide-beam radiation pattern.

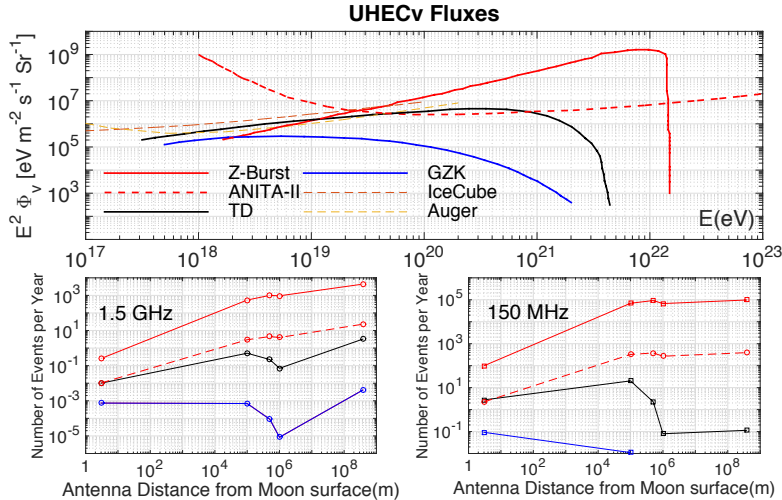


Figure 7: Top, Predicted fluxes for GZK neutrinos (Engel et al., 2001), Topological Defects (TD) and Z-Burst processes (Semikoz and Sigl, 2004). Also limits of recent neutrino observations: ANITA-II (Gorham et al., 2010), Auger (Aab et al., 2015) and IceCube (Aartsen et al., 2013a). Bottom, the expected events for a 1-year observation of lunar UHECv events. Event rates are for observations at 1.5 GHz (left) and 150 MHz(right) and are plotted vs. distance of the antenna from the Moon.

4. Categorization of Lunar UHECRv Events

The categorization of UHECRv events presented in this study is aimed at pre-data processing and event triggering. This is particularly important for lunar missions where data reduction is unavoidable due to the limitations on the data transmission to the Earth. The full analysis of events including particle composition and energy of events will be done in post-processing and offline data analysis when data is received on Earth. For onboard processing, digital beamforming and direction of arrival (DoA) techniques are used for detection of the events.

4.1. Low Energy/ High Energy Events

An estimate of CR flux between 10^{15} eV to 10^{18} eV is calculated from the CR flux spectrum (Aartsen et al., 2013b). This energy range in the spectrum is important because it is located between the regions known as Knee and Ankle and represents the transition between galactic and extragalactic cosmic rays. Due to the relatively low energy level of cosmic rays at this window, the only antenna on the lunar lander would be able to detect these events. We extend the calculation for apertures of lunar lander antenna at this region for both frequencies of 150 MHz and 1.5 GHz. It is found that with B.W. of 500 MHz at $f_o = 1.5$ GHz and B.W. of 50 MHz at $f_o = 150$ MHz, detection of 3 and 5 lunar CR events per year would be expected at this

region. Corresponding flux densities and apertures are illustrated in Fig.9. Although this is an interesting science case for a lunar lander experiment, still distinguishing these low energy events remains unsolved. In the next section, the propagation of the Askaryan radiation in the lunar regolith is studied.

4.1.1. Electric Fields of Askaryan Radiation for Cascade Showers

We analyze the propagation of Askaryan radiation in the lunar regolith. By solving Maxwell's equations in a dielectric medium such as the lunar regolith one can find the variation of the radiated signal versus time and location. Similar to (Hu et al., 2012), an illustration of the analysis of the Askaryan radiation in the lunar regolith is shown in Fig.10. J_z and J_r are the vertical and radial components of the current density. The current is due to the impact of the energetic particles. $E(r,z,t)$ represents the variation of the Electric field in space and time. For Askaryan radiation the equations can be simplified as follows: In this analysis cylindrical coordinates centred about the cascade are chosen to adjust for longitudinal and radial components. The lunar regolith is assumed to be homogenous and the cascade shower is symmetrical about the shower axis, therefore, the dependency on ϕ disappears in Maxwell's equations.

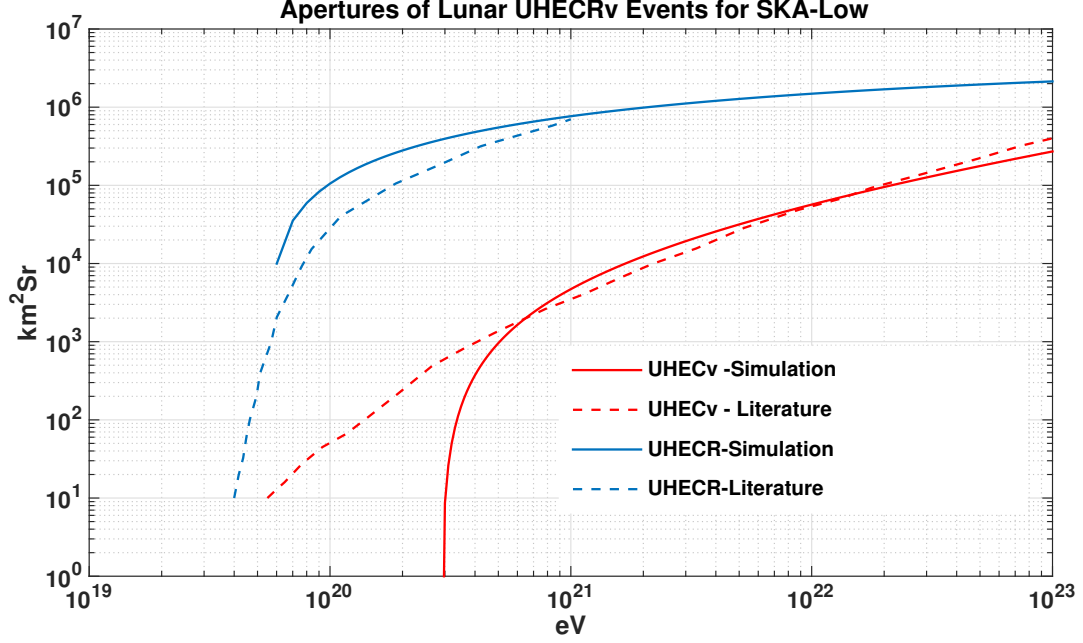


Figure 8: Simulation of lunar UHECRv apertures (solid curves) for SKA-Low using parameters in table 2. Results are compared with the existing models (dashed curves) in (Bray et al., 2014).

Furthermore, Askaryan radiation is highly linearly polarised (e.g. (Saltzberg et al., 2001)). Therefore its electric fields have components only in the radial direction and along the shower axis. This would eliminate E_ϕ and magnetic field components of H_r and H_z so the Maxwell equations reduce to (e.g. (Hu et al., 2012)):

$$\begin{aligned}
 -\partial H_\phi / \partial z &= \epsilon \cdot \partial E_r / \partial t + \sigma \cdot E_r \\
 1/r \cdot (\partial(r H_\phi) / \partial r) &= \epsilon \cdot \partial E_z / \partial t + \sigma \cdot E_z \\
 \partial E_r / \partial z - \partial E_z / \partial r &= -\mu \cdot \partial H_\phi / \partial t
 \end{aligned}
 \tag{5}$$

Where ϵ is the dielectric permittivity and μ is the magnetic permeability and σ is the conductivity of the lunar regolith. The general solution to above equations can be written as separable functions

(Jackson, 1998):

$$H_\phi(r, z, t) = f_1(r) \cdot f_2(z) \cdot f_3(t)$$

$$f_3(t) = \exp(j\omega t)$$

$$f_2(z) = \exp(-\gamma z)$$

$$\gamma = \alpha + j\beta$$

(6)

Where ω is the angular frequency, α is the attenuation constant, $\beta = 2\pi/\lambda$ is the propagation constant and

$$f_1(r) = c_1 \cdot J_1(K_1 r) + c_2 \cdot Y_1(K_1 r)$$

c_1 and c_2 are constants and $J_1(K_1 r)$ and $Y_1(K_1 r)$ are Bessel's functions of the first kind and second kind, respectively.

Considering the Eq.5 and the derivatives of the Bessel's functions as:

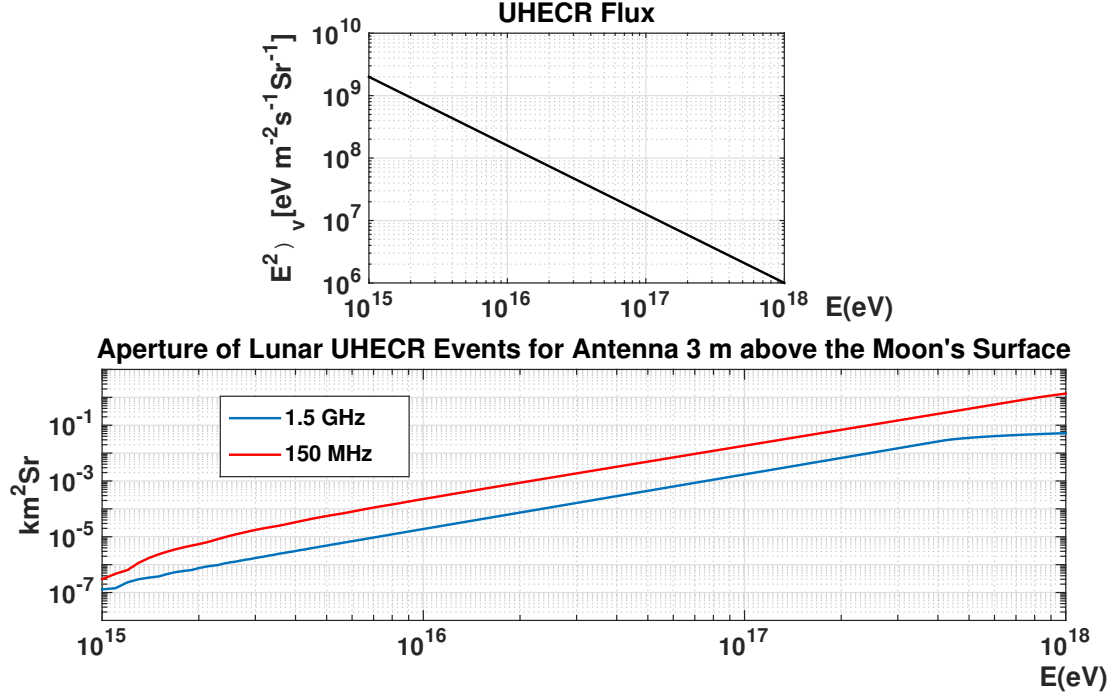


Figure 9: Lunar CR apertures at lower energies of 10^{15} eV to 10^{18} eV for antenna 3 m above the Moon's surface. Apertures are calculated for frequency of 1.5 GHz (B.W. of 500 MHz) and frequency of 150 MHz (B.W. 50 MHz). The CR flux (Aartsen et al., 2013b) is estimated between 10^{15} eV to 10^{18} eV. Using one antenna, the detection of 3 (1.5 GHz) and 5 (150 MHz) CR events per year is expected for this range of energy.

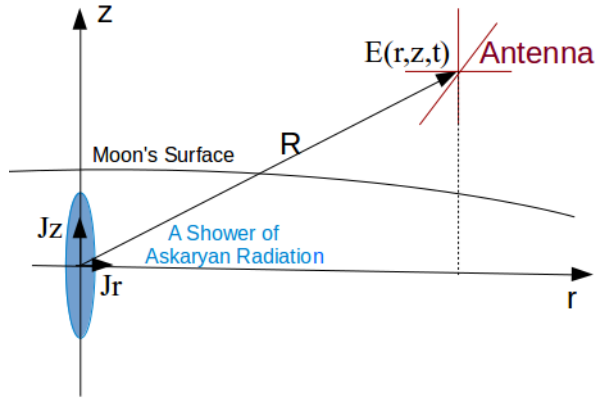


Figure 10: An illustration of the analysis of Askaryan radiation in the lunar regolith. J_z and J_r are the vertical and radial components of the current density. The current is due to the peak radio emission generated at the impact point of the energetic particles. $E(r,z,t)$ represents the variation of the electric field in space and time.

$$\begin{aligned}
 \partial J_1(r)/\partial r &= J_0(r) - J_1(r)/r \\
 \partial J_0(r)/\partial r &= -J_1(r) \\
 \partial Y_1(r)/\partial r &= Y_0(r) - Y_1(r)/r \\
 \partial Y_0(r)/\partial r &= -Y_1(r)
 \end{aligned} \tag{7}$$

The dependence of E_z to r is also a sum of the Bessel's functions as:

$$g(r) = c_3 \cdot J_0(K_1 r) + c_4 \cdot Y_0(K_1 r)$$

By solving Eq.5, E_r and E_z become:

$$E_r = \gamma / (j\omega\epsilon + \sigma) \cdot \exp(-\gamma z) \cdot \exp(j\omega t) \cdot f_1(r)$$

$$E_z = \exp(-\gamma z) \cdot \exp(j\omega t) \cdot g(r) \tag{8}$$

and K_1 is obtained as:

$$K_1 = (\omega^2 \cdot \mu \cdot \epsilon + \gamma^2 - j\omega \cdot \mu \cdot \sigma)^{0.5}$$

The exact solution of E_r and E_z depends on source excitement, boundary conditions and electromagnetic properties of the medium (ϵ , μ and σ). The constants in the above equations are identified with these conditions. In addition, the fields should be physically acceptable so that fields should have finite values at $r,z=0$ and at $r,z \rightarrow \infty$. Equations 8 provide a general picture of the behaviour of the fields in time and space in a dielectric medium (e.g. lunar regolith) when a cascade shower occurs. The electric fields propagate along the shower axis and are attenuated exponentially. The radial variation of the electric field is identified by Bessel's function where decaying field waves develop inside the lunar regolith. The details of a general solution to Maxwell's equations for this symmetrical geometry can be found in the literature. (e.g. (Smirnov and Valovik, 2013)).

4.2. Distinction of UHECRv Events in the Lunar Environment

From the aperture analysis in section 3, it is understood that downward UHECRv events have the most contribution in detectable cascade showers on the lunar surface. As discussed in the literature (e.g. (Jaeger et al., 2010)), Cherenkov cones are created by UHECRv travelling near-parallel to the Moon's surface. These UHECRv are not affected by total internal reflection so can partially escape the lunar regolith. This is the area where the Askaryan radiation becomes detectable by antenna so it is important that the antenna has horizontal elements parallel to the Moon's surface. If a tripole antenna is used, two crossed dipoles antenna could be positioned in a horizontal plane parallel to the lunar surface. The third vertical element would be also required for the total 3D coverage of space and would be used for DoA estimation and calibration. When the Earth is within the line of sight of the antenna, the radiation from Earth is received in the horizontal plane so it is indeed advantageous that 2 out of 3 dipole elements are positioned in horizontal plane (maximum of the radiation pattern at the zenith) to avoid radio-frequency interference (RFI) as much as possible.

For DoA measurement, a 3D coverage of space is required. This can be done using 3 orthogonal antenna elements to detect x, y and z component of

arrival signal. If the antenna is positioned on a moving platform, which is the case for antennas onboard a lunar orbiter, full Stokes parameters need to be calculated to obtain DoA and polarization of arrival signal. ((Cecconi and Zarka, 2005)). In general, arrival signals have components in 3 dimensions. However, UHECRv radiation is highly linearly polarised and one or two components might be missing so the second set of an antenna in a different position is highly desirable to localise the received signals. Such a basic radio interferometer can provide a degree spatial resolution (Aminaei et al., 2014).

Various radio signals are detectable in the lunar environment. In table 4 common radio emissions in the lunar environment are compared with radiation of UHECRv events. Impact of lunar dust, charged particles, and micro-meteorites generate radio pulses which cover a broad range of spectrum from kHz to GHz regime (Grimalsky et al., 2004). It has local peaks at kHz regime which are detectable by the antenna, Dust camera, and Langmuir probe (Klein-Wolt et al., 2012). Those events occurring near the antenna generate pulses which could be confused with UHECRv events for the lunar surface observations. Radio emission from planets (e.g. Jupiter and Saturn) peaks at frequencies up to 40 MHz (Gurnett et al., 2004) and solar bursts have a broad frequency spectrum up to GHz band. These point sky sources can be localised by beamforming. Terrestrial noise includes Auroral Kilometric Radiation (AKR in kHz band) and man-made RFI (kHz-MHz-GHz bands). Their effect is maximised on the Earth's visibility and should be removed by filters and post-data processing. Also, the data should be extracted from the Galactic background noise which is the global dominant noise in MHz band. Considering these types of radio emission in the lunar environment, the importance of triggering the UHECRv events can be understood better. Meanwhile, it should be emphasized that comparing to the Earth-based observation, the Moon enjoys much less man-made RFI and it lacks an ionosphere preventing ionospheric blockage and signal dispersion. Therefore, the lunar surface is a favorite platform to observe UHECRv events.

5. Technical Requirements of Future Lunar Radio Experiments

In this section, we present the basic system requirements of a radio detector for lunar UHECRv events. It is based on the receiver parameters of our analysis which has been compared with those of large radio array such as LOFAR (Scholten, 2007) and SKA (Bray et al., 2014) in tables 1 and 2. While for ground-based observation, the effects of ionosphere could be the main challenge, for space-based observation, the supplying power and data transfer to the Earth will be the main issues. Here we focus on the system requirements of space-based radio detectors. For that, we start with the preliminary design planned for LRX system and briefly present the recent developments of space-based radio astronomy. Furthermore, we discuss how the findings of this article might be applied to the system design of future lunar experiments. Fig.14 shows the block diagram of a basic space-based radio experiment including the antenna, analog electronics, power supply, data acquisition and data pre-processing unit. Data post-processing will be done in the ground-based stations for transmitted data. Power Supply Unit (DC-PSU) provides the required power in terms of DC voltage for the active components of analog and digital units. DC-PSU typically consists of rechargeable batteries which are charged by solar panels. It also includes Power Distribution Unit, DC-PDU, and DC-DC Converters.

5.1. Antennas and Analog Electronics

According to Eq. 1, the system sensitivity depends on the antenna collecting area and the bandwidth. Antenna collecting area can be increased by including more antennas in the array. It should be noted that an increase of the length of individual antenna elements would affect the performance of antenna and would create side-lobes in the radiation pattern.

Although by increasing the bandwidth, the receiver sensitivity is improved but the bandwidth is limited by antenna characteristics. Ideally antenna should have an omnidirectional pattern with the minimum side-lobes over the whole bandwidth to create the maximum aperture on the Moon's surface. If a resonance antenna is used the standard filters and amplifiers can be used and a matching network is not required. For 150 MHz, resonance (half-wavelength) dipoles with the length of 1m can

be used in a tripole structure. For broadband observations at high frequencies, log periodic antennas can be used. For instance, Lunar Orbital Radio Detector (LORD) has two circularly polarized log-periodic spiral antennas for UHECRv observations in a spectrum window of 200-800 MHz. LORD is planned to operate on a polar lunar orbiter spacecraft at 100-150 km altitude for one year and then at 500-700 km for two years (Raybov et al., 2016). Here we present a one antenna candidate for each frequency regime. For 150 MHz, a tripole antenna which consists of three orthogonal dipoles would be a good choice. The length of a resonance dipole at 150 MHz is 1 m which is comparable to the dimension of a lunar lander or lunar orbiter satellites. Therefore the radiation pattern could be affected if the antenna is mounted on a lunar lander or on a satellite. Here a simple analysis of a tripole antenna above the Moon's surface is presented. Simulation is done using cocoaNEC 2.0 software (Chen, 2012). The far-field radiation pattern of a tripole antenna in the presence of lunar regolith is illustrated in Fig. 11. The total length of each arm is 1m (resonance antenna at 150 MHz) and the 3 dipoles are feed in the centre with for antennas 2 and 3 of the tripole are offset by 45 degrees phases (voltage sources of $1\angle 0^\circ$ V, $1\angle 45^\circ$ V, $1\angle -45^\circ$ V). The centre of the tripole is 1 m above the Moon's surface (half wavelength at 150 MHz). This set up generates a wide beamwidth as shown in Fig. 11. The Voltage Standing Wave Ratio (VSWR) of this antenna is illustrated in Fig. 12 which shows the best matching at 150 MHz with VSWR of 2.21. By increasing the length and the distance of antennas from the lunar regolith, side-lobes appear in the radiation pattern. Adding a limited ground plane to the simulated antenna using radial wires of the length of 2m improves the VSWR to 1.71 but the beamwidth reduces. An antenna with limited ground-plane could represent the antenna onboard a lunar lander or lunar satellite orbiter, the dimension and materials of the body of the lander/satellite, however, should be known for exact radiation pattern simulation. The near-field radiation pattern of a tripole antenna in the presence of lunar regolith is illustrated in Fig. 13. The antenna has the same set up as for the far-field and simulation is done using XNEC2c Antenna Software (Kyriazis, 2005). The near-field radiation pattern and the variation of the electric field in the near-field from 0.5 m up to 4 m distance from the tripole is shown in the figure. Also the current distribution across the dipole arms has been shown

using colorbars. It can be seen that the near-field radiation pattern is similar to the far-field pattern although the max. gain is slightly higher for near-field patten(4.25 dBi comparing to 3.81 dBi).

For antennas onboard lunar satellites at 1.5 GHz, a helical antenna can be used. Using the formula of a helical antenna in (Kraus and Marhefka, 2002) the basic parameters of a helical antenna in the presence of a ground plane with dimension of at least 2 wavelengths is calculated. The antenna dimensions (in GHz band), its circular polarization and half-power beamwidth (HPBW), make helical antenna a good choice for an antenna onboard a lunar orbiter satellite for detection of UHECRv events. At 1.5 GHz, a ground plane with dimension of $2\lambda = 40$ cm and bigger is suitable, which can be fairly approximated with the body of a satellite with this size. For smaller ground planes, the radiation pattern would partially be scattered. The typical helical antenna parameters are summarized in table 5. At 1.5 GHz, such an antenna has a circumference of 0.2 m with 5 turns and spacing of 4 cm between turns. The 3dB bandwidth of the antenna is 320 MHz, about 20% of the central frequency. The antenna operation mode is axial mode and the polarization is circular which can detect both quasi-horizontal and vertical events. The HPBW is 52 degree which covers the entire lunar aperture for a lunar orbiter experiment at 1000 km distance. The antenna input impedance of 140Ω corresponds to VSWR=2.77 which can be improved by using a matching impedance. For localisation of the events, at least three individual antenna is required. Localisation is part of the event detection and initially excludes other lunar radio emission which is not occurring in the lunar regolith from the likely UHECRv events. The analog electronics typically include analog filter and low noise amplifier. If the receiver is exclusively designed for UHECRv detection a band-pass filter is preferred. This will remove the unwanted radiations outside the selected window. For instance, for a 150 MHz observation using a resonance antenna, a bandwidth of 20 MHz is expected. For observations at low frequencies resonance antenna might not be used due to the long length, therefore a matching network would be required. Since matching network limits the system bandwidth, non-matched dipoles have been proposed for broadband observations (Arts et al., 2010), (Rajan et al., 2016).

For broadband receivers, a filter after amplifier is needed to remove the components of harmonics gen-

erated in the amplifier. The gain of the amplifier varies based on the gain of the antenna and the distance of antenna from the Moon's surface. Since antenna gain in space-based UHECRv experiments is ideally low, the gain of the amplifier is rather high (more than 20 dB) so the amplifier might be designed in 2-3 stages. This is to meet the receiver sensitivity requirements e.g. the minimum signal level required for the ADCs (analog-to-digital converters).

5.2. Data Acquisition and Data Processing Unit

The digital unit includes the data acquisition (DAQ) and Data Processing Unit (DPU). The amplified signal is digitized by ADCs. The ADC sampling rate should meet the Nyquist limit ($f_s \geq 2f_0$) which f_s is the sampling frequency and f_0 is the frequency of observation. 10-bit ADCs are planned for LORD Experiment with f_s of 2 Gbps (Raybov et al., 2016). The dynamic range of the digital receiver can be improved by adding more bits to ADCs at the expense of additional processing time and power consumption. For each run of data taking, the ADC is calibrated and the level of input signal is adjusted by a gain controller. In addition to Discrete Fourier Transform (DFT) or cross-correlation between input channels, the digitized data can be channelised in the frequency domain. This, for instance, can be done using a Polyphase Filter Bank(PFB) which has been suggested for a distributed space-based radio array (Rajan et al., 2016). Compared to DFT, PFB is more complex and roughly costs 1.5 times more but it produces a relatively flat response across the channels and prevents the leakage of the signals in the nearby channels (Chennamangalam, 2014). This factor is particularly important for RFI Mitigation (RFIM) while detecting weak astronomical signals. It, however, has been argued (Bray et al., 2014) that detection of a UHECRv radio pulse in the order of nanoseconds is problematic after PFB as it splits the radio signals over the multiple frequency bands. In order to prevent that, an invert PFB process with a minor loss of efficiency can be applied to restore the time domain signal for each beam (Singh et al., 2012). Alternatively, a pre-selection of events can be achieved before PFB in time series data. For instance, digitized time-series data is sent to a temporary memory, the buffer unit (Fig. 14). Depending on the duty cycle of the antenna, the main data stream could

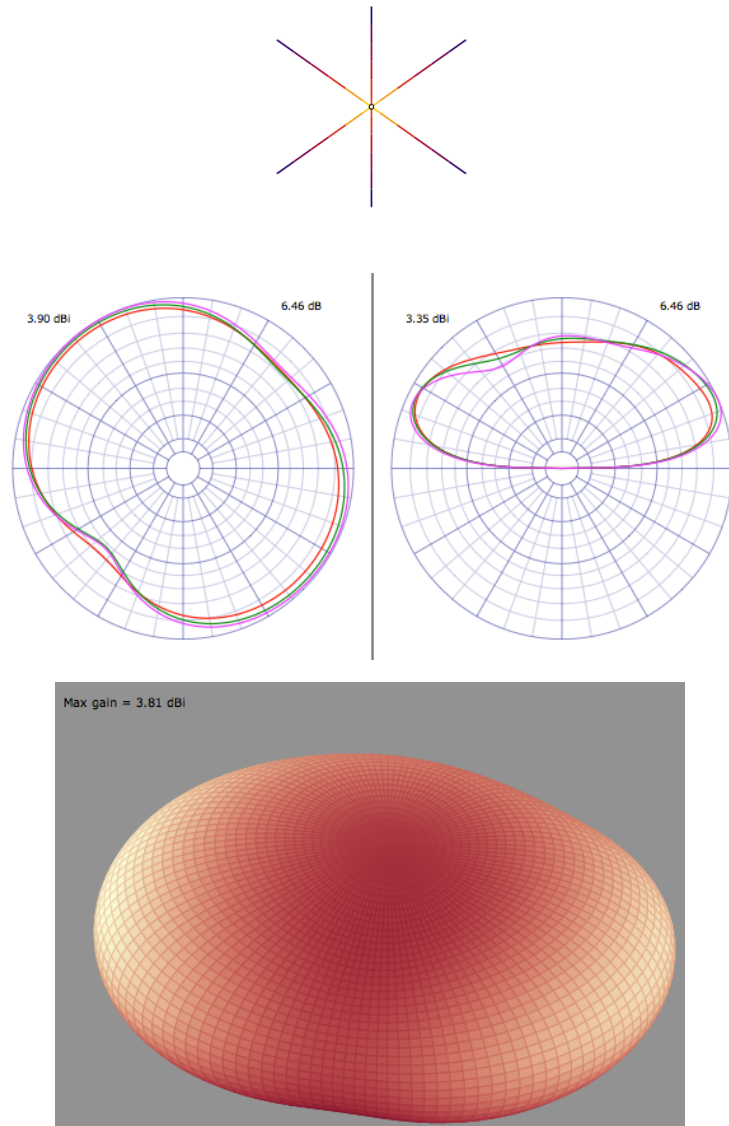


Figure 11: Top, the variation of current in tripole arms. The central feed excitations are $1 < 0$ degrees V, $1 < +45$ degrees V and $1 < -45$ degrees V. Bottom, radiation pattern in azimuth (left) and elevation planes. Also the 3D radiation pattern of the tripole in the presence of lunar regolith. The centre of the antenna is 1 m above the Moon's surface and the total length of each dipole is 1 m. Simulation is done using cocoaNEC 2.0 software(Chen, 2012)

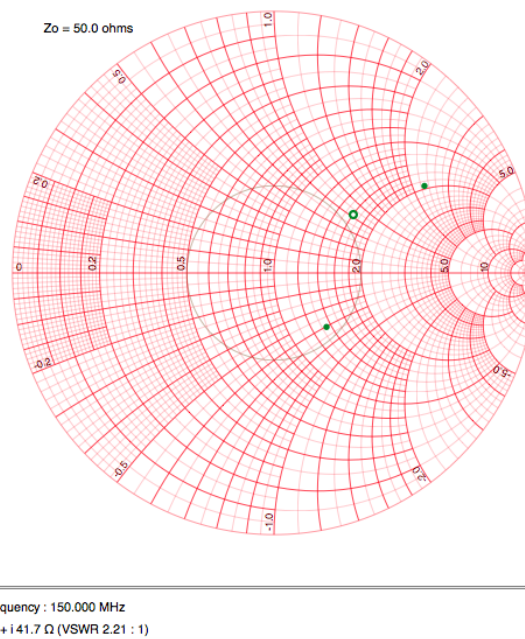


Figure 12: An illustration of the Smith Chart for the input impedances and VSWR of the tripole antenna in Fig. 11. Green points are the normalized impedances of 140 MHz, 150 MHz and 160 MHz (top). Numbers along the diameter of the biggest circle resemble the normalised resistance. Numbers around the biggest circle resemble the normalised reactance. Number 1 at the centre resembles the VSWR =1 for the perfect antenna impedance matching. The analysis is done using cocoaNEC 2.0 software (Chen, 2012)

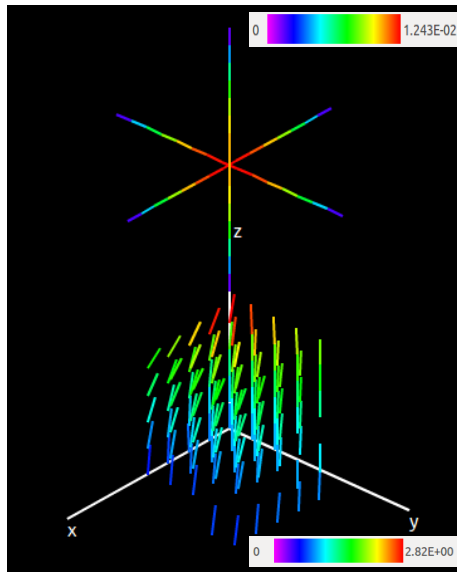
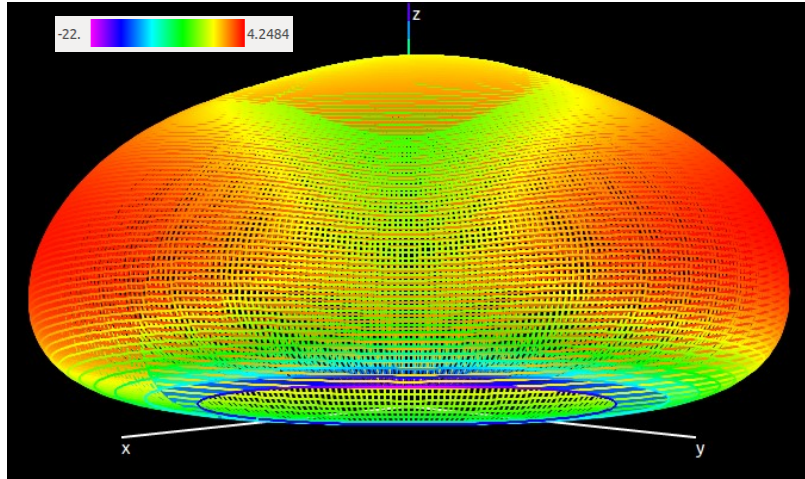


Figure 13: Top, simulation of near-field radiation pattern (in dB) of a tripole antenna at 150 MHz in the presence of lunar regolith. Bottom, variation of current in tripole arms. The central feed excitations are $1 \angle 0^\circ$ degrees V, $1 \angle +45^\circ$ degrees V, and $1 \angle -45^\circ$ degrees V. Also the variation of electric field in the near-field from 0.5 m up to 4 m distance from the tripole. The total length of each dipole is 1 m. Color code on the top is for the antenna current distribution (A) and the one on the bottom shows the variation of the electric field (V/m). Simulation is done using XNEC2c Antenna Software. (Kyriazis, 2005)

generate a large volume of data but only those selected by the trigger are stored and sent for processing. For a distributed antenna array, data is synchronized using precise onboard clocks. For a single tripole antenna, a common onboard clock for 3 input channels would be needed while for a distributed space-based array, each satellite needs a clock. The choices of space-qualified clocks for such an array are introduced in (Rajan et al., 2016). It has been also discussed that in the presence of RFI, the Effective Number Of Bits (ENOB) should be greater than 12. For an observing frequency of 150 MHz, this matches to a Signal to Noise Ratio (SNR) around 60 dB and requires a jitter timing of 1 ps and smaller (Rajan et al., 2016). This makes the detectable signal well above the noise level and the likely events can be triggered. Data correlation and Pre-beamforming can be achieved at this stage along with RFI mitigation. Various methods of analog and digital beam-forming and a combination of both analog and digital in a multipoint Butler Matrix have been proposed for space communications which also can be used for multi-beam radio telescopes. For instance, a fully reconfigurable Beam-Forming Network can be done using $M \times N$ control elements of the variable phase shifters and attenuators. The network generates N independent beams from M inputs of antenna elements (Angeletti and Lisi, 2013). In parallel to the channelised data (in the frequency domain), snapshots of time series data can be sampled and those corresponding to the selected events will be stored (Klein-Wolt et al., 2012). The Earth's transfer data rate is usually very limited and varies between tens of kbps to few Mbps (e.g. (Rajan et al., 2016)) depending on the Earth visibility and link budget parameters. The volume of stored data can be reduced by compression techniques in the data processing unit before data is sent to the Earth. For lossless compression, the compression ratio of 10 and higher has been reported for space missions (CCSDS, 2013).

6. Summary and Conclusion

We examine the possibility of a radio detection of lunar UHECR ν events in two frequency regimes a 150 MHz and a 1.5 GHz. For the selected frequencies, the analytical method is reliable for the whole range of energy ((Gayley et al., 2009), (Jeong et al., 2012)).

For future lunar missions, we ran a simulation using

a single antenna at different distances from the lunar surface and compared the results with ground-based observations. The method can be applied to an array of antennas on the Moon's surface or multiple antennas onboard lunar orbiters. The results show that the size of UHECR ν aperture depends roughly on the square of the wavelength of observation. Therefore the chance of detecting UHECR ν events significantly increases in the MHz regime. For the system requirements, the size of the antenna depends on the wavelength of the observation so the antenna will be shorter in GHz regime. However, for the digital receiver, the sampling rate of digitizer depends on the frequency bandwidth which makes the digital processing in the GHz band more complicated. Due to the large volume of digitized data in GHz band, data transfer to the Earth could be particularly problematic for ongoing lunar missions. Lunar UHECR ν events in the low-frequency regime (kHz to few MHz) are also possible and are likely to be influenced by transition radiation as opposed to charge excess mechanism for the MHz and GHz bands. kHz observation, however, is not practical for lunar missions due to the size of antennas to be deployed in space or on the lunar surface.

For selected frequencies, the expected event rates (Fig.4, Fig.7) for cosmic rays, GZK neutrinos and TD neutrinos are consistent with the previous numerical and analytical simulations in the literature ((Gusev et al., 2006), (Stål, 2007), (Gayley et al., 2009), (Jeong et al., 2012)). However, the expected event rate for Z-Burst cosmic neutrinos shows a significant reduction after applying the limits of recent observation (ANITA II, (Gorham et al., 2010)). This predicts roughly fewer Z-Burst neutrino events by 2 orders of magnitude for both frequencies. For detection of lunar GZK neutrinos, an array of hundreds of antennas on the Moon's surface seems to be the most probable choice, while for higher energy levels (e.g. TD Neutrinos and Z-Burst Neutrinos), lunar orbiter experiments at distances of 500-1000 km would provide the optimum position to observe lunar UHECR ν events.

We also evaluate the possibility of the detection of neutrinos in the lunar sub-regolith by calculating UHECR ν apertures. In this paper, we take this into account only for lunar observation at 3 m distance from the lunar surface, and find that an additional contribution of 50% to 60% is expected from the sub-regolith.

Our preliminary study shows that events occurring in sub-regolith are also detectable as far away as

Earth-based observations, since radiation attenuation is very low in the lunar regolith and sub-regolith. This would be an interesting topic for future study to apply electromagnetic properties of the lunar environment in relation to the detection of Askaryan radiation due to the impact of UHECRv.

We also investigate the propagation of Askaryan radiation in the lunar regolith. Assuming that the shower cascade generates upward and radial components of the current density, the electric fields will be decaying exponentially while propagating towards the Moon's surface. The radial propagation with a pattern of Bessel's functions. Fig.15 illustrates a summary of lunar UHECRv radio experiments and the effective parameters.

Appendix A. Calculation of the UHECRv Apertures

Here are the modifications made to the analytical methods used in (Gayley et al., 2009) and (Jeong et al., 2012) for this paper. The main difference is that for Earth-based observations the full Moon's surface is assumed to be illuminated by the antenna, while for lunar orbiters and lunar lander observation only a portion of Moon's surface can be illuminated by the antenna. As opposed to Earth-based observations, the antenna distance from the Moon's surface is comparable to the radius of the illuminated area. Therefore for the illuminated area, the antenna distance is variable. The total aperture (Ap) is then calculated by integrating the illuminated area and probability function of the occurrence of UHECRv events over the maximum radius that antenna can illuminate the Moon's surface. The details are illustrated in Fig.A.16 where

$$R_{ap} = R_{moon} \cdot h / (R_{moon} + h) \cdot [(1 + 2(R_{moon}/h))^{0.5}]$$

$$Ap(E, f, R_{ap})_{CRv} = \int_0^{R_{ap}} A_0(r) \cdot P(E, f, r) dr$$

(A.1)

f is frequency and $A_0(r)$ is the area on the Moon's surface with radius (r) that is illuminated with antenna radiation beams. $P(E, f, r)$ is a complex function of the probability of the occurrence

of UHECRv and UHECR events which are adapted from (Gayley et al., 2009) and (Jeong et al., 2012) respectively. $P(E)$ UHECRv for various distances from the lunar surface and at both frequencies of 150 MHz and 1.5 GHz are plotted in Fig.A.17 For calculation of aperture of UHECRv events for lunar lander observation, the effect of sub-regolith is also taken into account.

$$Emax_{Reg.} = 0.0845 \cdot (10^{-6}(1/d) \cdot (Es) \cdot (f_{GHz}) \cdot 10^{-18}) \cdot (1 + ((f_{GHz})/2.32))^{-1.23}$$

$$Emax_{sub} = 0.0569 \cdot (10^{-6}(1/d) \cdot (Es) \cdot (f_{GHz}) \cdot 10^{-18}) \cdot (1 + ((f_{GHz})/2.38))^{-1.23}$$

Where:

$$E_{sub} = att \cdot Emax_{sub}$$

$$Es = 0.2 \times E(eV) \quad \text{for Neutrinos}$$

$$tan\delta = 0.01 \quad \text{Loss Tangent}$$

$$\epsilon = 3 \quad \text{Dielectric Constant for Moon}$$

$$\lambda = 3 \times 10^8 / f \quad \lambda \text{ is Wavelength of Observation}$$

$$Ds = \lambda / (\pi \cdot \delta \cdot (\epsilon)^{0.5}) \quad Ds : \text{Skin Depth}$$

$$h_{max} = 10 \text{ m} \quad \text{Thickness of Lunar Regolith}$$

$$att = exp(-h_{max}/Ds) \quad \text{Attenuation of Radiation}$$

(A.2)

Here $Emax_{Reg.}$ is the maximum electric field of Askaryan radiation generated in the lunar regolith. $Emax_{sub}$ is the maximum electric field of Askaryan radiation generated in the sub-regolith. The electric field of sub-regolith events at the antenna point (E_{sub}) is calculated with considering the attenuation due to the passage of the signal through 10 m regolith. f_{GHz} is the frequency of observation in GHz. $Emax_{Reg.}$ and $Emax_{sub}$ are taken from (James and Protheroe, 2009). $Emax$ is used in calculation of $P(E, f, r)$. The total aperture then becomes the sum of apertures of regolith and sub-regolith.

Acknowledgements

The work of L. Chen is supported by National Natural Science Foundation of China (11573043). We thank the ASR co-editor, Biswajit Paul, and two anonymous reviewers for their constructive comments, which improved the manuscript substantially.

Radio Emission	Characteristics	Dominant Frequency Spectrum
Lunar dust and charged particles	Nearby antenna surface emission	kHz
(Micro) Meteorites	Nearby antenna surface emission	MHz-GHz
Sky radio sources (Sun, Planets)	Strong point sources	kHz-MHz
Terrestrial noise (AKR,RFI)	On Earth visibility	kHz-MHz
Galactic background noise	Global emission	MHz
UHECR	Lunar surface(horizontal angles)	MHz-GHz
UHECv	Lunar surface and regolith	MHz-GHz

Table 4: Radio emission in the lunar environment

Typical parameters of a helical antenna in the presence of a ground plane

Frequency(F)	1.5 GHz	
Bandwidth (BW)	1348 MHz-1668 MHz	320 MHz
Number of turns(N)	5	
Spacing between turns(S)	0.2λ	4cm
Circumference of Helix (C)	λ	0.2m
Input Impedance	$140C/\lambda$	140 Ω
HPBW (Degrees)	$52\lambda^{1.5}/[C(NS)^{0.5}]$	52
Directivity	$15NC^2S/\lambda^3$	11.76dBi
Operation mode	Axial	Circular polarization

Table 5: Typical parameters of a helical antenna in the presence of a ground plane calculated (Kraus and Marhefka, 2002) for the central frequency of 1.5 GHz.

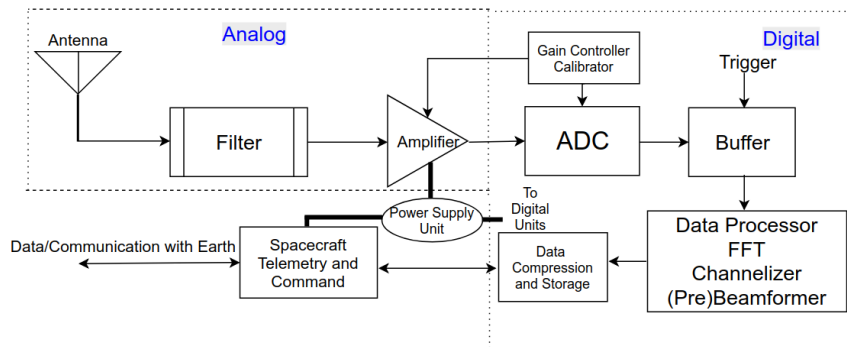


Figure 14: A block diagram of basic system requirements for a lunar UHECRv radio experiment

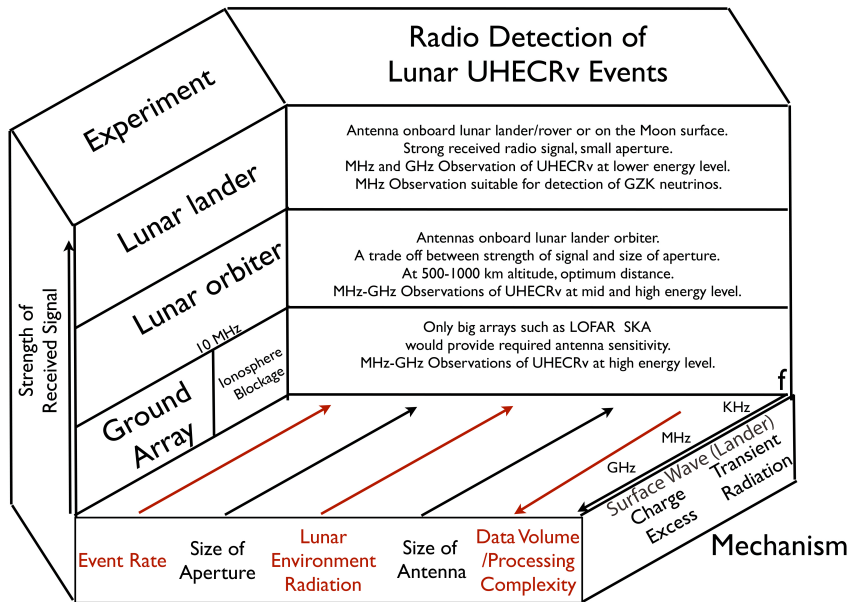


Figure 15: A flowchart of lunar UHECRv radio experiments

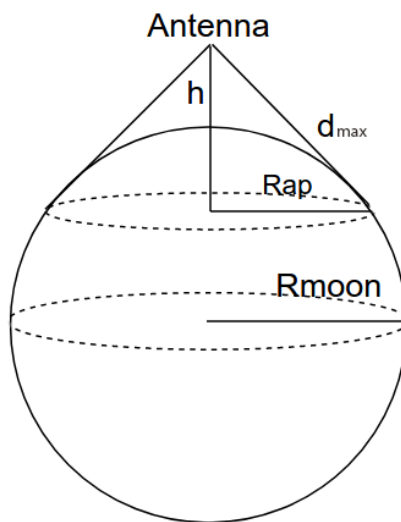


Figure A.16: An illustration of UHECRv aperture on the Moon's surface. R_{moon} : Radius of Moon (1738 km), h : Antenna distance from the Moon's surface, R_{ap} : Radius of Aperture, d : Maximum distance of antenna from Aperture

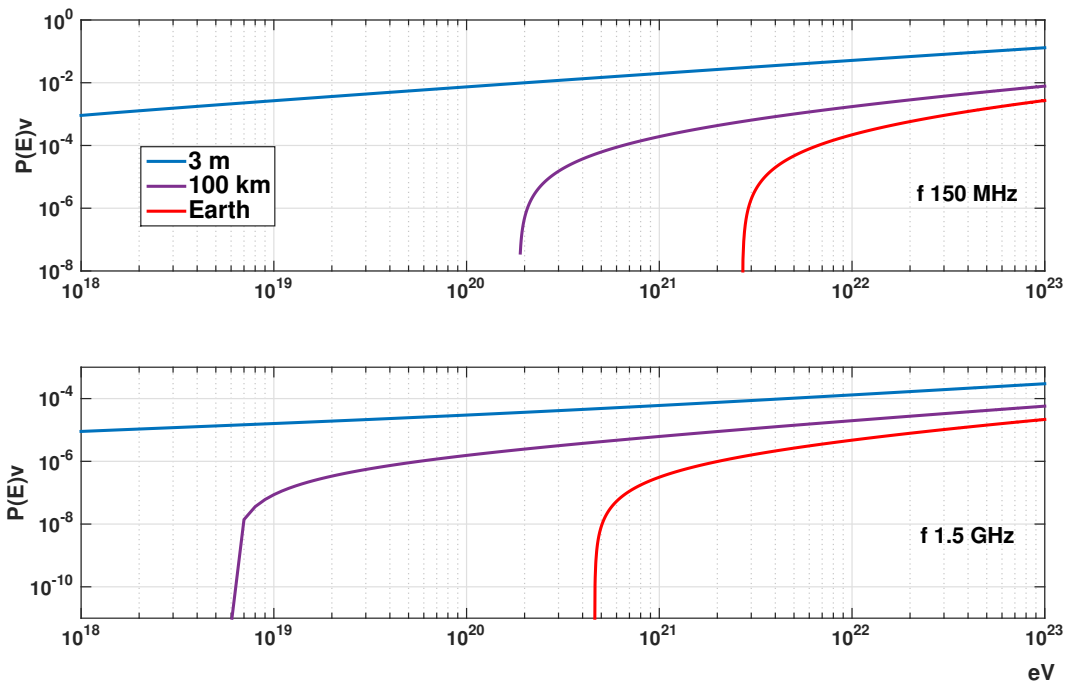


Figure A.17: The probability function, $P(E)$, of detection of UHECV events for lunar experiments at frequencies of 150 MHz (top) and 1.5 GHz. $P(E)v$ is plotted for antenna 3m above the Moon's surface (lander), 100 km (lunar orbiter) and Earth-based array. System parameters are shown in table 1 and table 2

References

- Aab, A., Abreu, P., Aglietta, M., et al., 2015. Improved limit to the diffuse flux of ultra-high energy neutrinos from the Pierre Auger Observatory, *Phys. Rev. Lett.* Vol. 91. p. 092008.
- Aartsen, M., Ackermann, M., Adams, J., et al., 2014. Observation of High- Energy Astrophysical Neutrinos in Three Years of IceCube Data , IceCube Collaboration, *Phys. Rev. Lett.* , 113, 101101.
- Aartsen, M. G., Abbasi, R., Abdou, Y., et al., 2013a. First observation of PeV-energy neutrinos with IceCube, *Phys. Rev. Lett.* Vol. 111. p. 021103.
- Aartsen, M. G., et al., 2013b. IceCube Collaboration, Measurement of the high-energy cosmic ray spectrum with IceTop-73, *Physical Review D* 88 . p. 042004.
- Abraham, J., Abreu, P., Aglietta, M., et al., 2010. Measurement of the energy spectrum of cosmic rays above 10^{18} eV using the Pierre Auger Observatory, The Pierre Auger Collaboration, *Phys. Lett.* B685. pp. 239–246.
- Aminaei, A., Klein-Wolt, M., Chen, L., et al., 2013. The Prospects of Radio Detection of UHECRv on the Moon's Surface, in *Proceedings of 33rd International Cosmic Ray Conference (ICRC)*, Brasil. pp. 3358, abstract number 0223.
- Aminaei, A., Klein-Wolt, M., Chen, L., et al., 2014. Basic radio interferometry for future lunar missions, *IEEE Aerospace Conference, Big Sky, MT, USA*. pp. 1–19.
- Angeletti, P., Lisi, M., 2013. A Digital Revisitation of Analog Beam-forming Techniques for Satellite Multibeam Antennas, *Conference Paper, 31st AIAA International Communication Satellite Systems Conference*. pp. 752–757.
- Arts, M., van der Wal, E., Boonstra, A.-J., 2010. Antenna concepts for a space-based low-frequency radio telescope, *ESA Antenna Workshop on Antennas for Space Applications, The Netherlands*. Vol. 32. pp. 5–8.
- Askaryan, G. A., 1965. Excess Negative Charge of an Electron-Photon Shower And Its Coherent Radio Emission, *JETP* 14, 441, 1962; also *JETP* 21, 658.
- Barwick, S. W., Beatty, J. J., Besson, D. Z., et al., 2006. Constraints on cosmic neutrino fluxes from the Antarctic Impulsive Transient Antenna experiment, ANITA collaboration, *Phys. Rev. Lett.* 96, 171101.
- Belov, K., Bechtol, K., Borch, K., et al., 2015. SLAC T-510: A beam-line experiment for radio emission from particle cascades in the presence of a magnetic field, in *Proceedings of 34th International Cosmic Ray Conference (ICRC)*, The Netherlands . p. 346.
- Bentum, M. J., Verhoeven, C. J. M., Boonstra, A. J., et al., 2009. A novel astronomical application for formation flying small satellites, In *60th International Astronautical Congress (IAC)*, Republic of Korea. pp. 1–8.
- Bhattacharjee, P., Hill, C. T., Schramm, D. N., et al., 1992. Grand unified theories, topological defects, and ultrahigh-energy cosmic rays, *Phys. Rev. Lett.* 69, 567.
- Bray, J. D., 2016. The sensitivity of past and near-future lunar radio experiments to ultra-high-energy cosmic rays and neutrinos, *Astropart.Phys.* 77. pp. 1–20.
- Bray, J. D., Alvarez-Muniz, J., Buitink, S., et al., 2014. Lunar detection of ultra-high-energy cosmic rays and neutrinos with the Square Kilometre Array (SKA), presented in *Advancing Astrophysics with the SKA, Italy*. p. 144.
- Carrier, W. D., Olhoef, G., Mendell, W., 1991. Physical properties of the lunar surface, in: G. Heiken et al. (Eds.), *Lunar Sourcebook: A User's Guide to the Moon*. Cambridge Univ. Press, New York. pp. 475–594.
- CCSDS, 2013. Lossless Data Compression, Consultative Committee for Space Data Systems (CCSDS) Report Concerning Space Data System Standards. Vol. 3.
- Cecconi, B., Zarka, P., 2005. Direction finding and antenna calibration through analytical inversion of radio measurements performed using a system of 2 or 3 electric dipole antennas, *Radio Science*, 40, RS3003.
- Chen, K., 2012. cocoaNEC Reference Manual, Open Source Antenna Software, Version 2.0.
- Chen, L., Aminaei, A., Falcke, H., et al., 2010. Optimized estimation of the Direction of Arrival with single tripole antenna, *Publication of Loughborough Antenna and Propagation Conference (LAPC)*, UK. pp. 93–96.
- Chennamangalam, J., 2014. The Polyphase Filter Bank Technique, The Collaboration for Astronomy Signal Processing and Electronics Research (CASPER), Memo 41.
- Dagkesamanskii, R., Zheleznykh, I., 1989. Radio-astronomy method for detecting neutrinos and other elementary particles of superhigh energy, *Phys. JETP* . Vol. 50. p. 259.
- Engel, R., Seckel, D., Stanev, T., 2001. Neutrinos from propagation of ultrahigh energy protons, *Phys. Rev. D* 64, 093010.
- Gayley, K. G., Mutel, R. L., Jaeger, T., 2009. Analytic Aperture Calculation and Scaling Laws for Radio Detection of Lunar-Target UHE Neutrinos, *ApJ* 706, 1156.
- Gorham, P., Liewer, K. M., Naudet, C. J., et al., 1999. Initial Results from a Search for Lunar Radio Emission from Interactions of 10^{19} eV Neutrinos and Cosmic Rays, in *Proceedings of the 26th International Cosmic Ray Conference, USA*. p. 2.HE.6.3.15.
- Gorham, P. W., Allison, P., Baughman, B., et al., 2010. Observational constraints on the ultrahigh energy cosmic neutrino flux from the second flight of the ANITA experiment, *Phys. Rev. Lett.* Vol. 82. p. 022004.
- Gorham, P. W., Hebert, C. L., Liewer, K. M., et al., 2004. Experimental Limit on the Cosmic Diffuse Ultrahigh Energy Neutrino Flux, *Phys. Rev. Lett.* 93 (4), 041101 .
- Grimalsky, V., Berezhnoy, A., Kotsarenko, A., et al., 2004. Interpretation of the microwave non-thermal radiation of the Moon during impact events, *Natural Hazards and Earth System Sciences*. Vol. 4. pp. 793–798.
- Gurnett, D., Kurth, W., Kirchner, D., et al., 2004. The Cassini Radio and Plasma Wave Investigation, *Space Science Reviews* . Vol. 114. p. 395–463.
- Gusev, G. A., Lomonosov, B. N., Pichkhadze, K. M., et al., 2006. Detection of ultrahigh-energy cosmic rays and neutrinos by radio method using artificial lunar satellites, *Cosmic Research*. Vol. 44. pp. 19–38.
- Hu, C.-Y., Chen, C.-C., Chen, P., 2012. Near-Field Effects of Cherenkov Radiation Induced by Ultra High Energy Cosmic Neutrinos, *Astropart. Phys.* Vol. 35. pp. 421–434.
- Horandel, J., Bahren, L., Buitink, S., et al., 2009. LOFAR - A new experiment to record radio emission from cosmic particles, *Nucl. Phys. B* . Vol. 196. p. 289.
- Jackson, J. D., 1998. *Classical electrodynamics*, Book, John Wiley and Sons, Inc., Third edition.
- Jaeger, T., Mutel, R. L., Gayley, K., 2010. Project RESUN, a Radio EVLA Search for UHE Neutrinos, *Astroparticle Physics* , Issue 5. Vol. 34. p. 293–303.
- James, C., Protheroe, R., 2009. The sensitivity of the next generation of lunar Cherenkov observations to UHE neutrinos and cosmic rays, *Astropart.Phys.* Vol. 30. pp. 318–332.

- James, C. W., 2013. A model for the effects of small-scale surface roughness on lunar pulse detection, in Proceedings of 33rd International Cosmic Ray Conference (ICRC), Brasil . p. 1052.
- James, C. W., Ekers, R. D., Alvarez-Muniz, J., et al., 2010. LUNASKA experiments using the Australia Telescope Compact Array to search for ultrahigh energy neutrinos and develop technology for the lunar Cherenkov technique , *Phys. Rev. D*, 81 (4), 042003 .
- James, C. W., Falcke, H., Huege, T., et al., 2011. General description of electromagnetic radiation processes based on instantaneous charge acceleration in endpoints, *Phys. Rev. E* 84, 056602.
- Jeong, Y. S., Reno, M. H., Sarcevic, I., 2012. Radio Cherenkov signals from the Moon: neutrinos and cosmic rays, *Astrop.Phys.*, 35(6), 383-395.
- Klein-Wolt, M., Aminaei, A., Zarka, P., et al., 2012. Radio astronomy with the Lunar Lander: opening up the last unexplored frequency regime, P&SS, in the special issue SPME. pp. 167–178.
- Kraus, J. D., Marhefka, R. J., 2002. Antennas for all Applications, 3rd Edition, USA: McGraw-Hill .
- Kyriazis, N., 2005. Xnec2c User Manual, Open Source Antenna Software, Version 2.3-beta.
- Marfatia, D., McKay, D., Weiler, T. J., 2015. New physics with ultra high energy neutrinos , *Phys. Lett. B.*, 748. pp. 113–116.
- Mercurio, B., 2009. A simulation of the ANITA experiment with a focus on secondary interactions, Dissertation, The Ohio State University.
- Nan, R., Li, D., Jin, C., et al., 2011. The Five-Hundred-Meter Aperture Spherical Radio Telescope (FAST) Project, *Int. J. Mod. Phys. D* 20, 989.
- Oberoi, D., Pinçon, J.-L., 2005. A new design for a very low frequency spaceborne radio interferometer , *Radio Science*, Vol. 40, RS4004.
- Olhoeft, G. R., Strangway, D. W., 1975. Dielectric Properties of the First 100 Meters of the Moon, Earth and Planetary Science Letters. Vol. 24. pp. 394–404.
- Pugacheva, S. G., Shevchenko, V. V., 2000. The Model of The Moon's Thermal Radiation in the Infrared Spectral Ranges (10-12 micron), in 31st Lunar and Planetary Science Conference, USA. p. abstract number 1129.
- Rajan, R. T., Boonstra, A.-J., Bentum, M., et al., 2016. Space-based aperture array for ultra-long wavelength radio astronomy, *Experimental Astronomy*. Vol. 41. pp. 271–306.
- Raybov, V. A., Chechin, V., Gusev, G. A., et al., 2016. Prospects for ultrahigh-energy particle observation based on the lunar orbital LORD space experiment, *Advances in Space Research*. Vol. 58. pp. 464–474.
- Saltzberg, D., Gorham, P., Walz, D., et al., 2001. Observation of the Askaryan Effect: Coherent Microwave Cherenkov Emission from Charge Asymmetry in High Energy Particle Cascades, *Phys.Rev.Lett.* 86 , 2802-2805 .
- Scholten, O., 2007. Optimal Radio Window for the Detection of Ultra-High-Energy Cosmic Rays and Neutrinos off the Moon, *J. Phys.: Conf. Ser.* 81 012004.
- Scholten, O., Buitink, S., Bacelar, J., et al., 2009. First results of the NuMoon experiment, *Nucl. Instr. and Meth. V* 604, S102.
- Semikoz, D. V., Sigl, G., 2004. Ultra-high energy neutrino fluxes: new constraints and implications, *J. Cosmol. and Astropart. Phys.* 04. 003.
- Shoemaker, E. M., Morris, E. C., 1969. Thickness of the regolith., in *Surveyor: Program results*, NASA Special Paper 184. Washington D.C, U.S. Government Printing Office. pp. 96–98.
- Singh, K., Mevius, M., Scholten, O., et al., 2012. Optimized trigger for ultra-high-energy cosmic-ray and neutrino observations with the low frequency radio array. Vol. 664. Elsevier BV, pp. 171–185.
- Sinha, K., Datta, P., 2012. Transition radiation as a tool for radio detection of Ultra High Energy Neutrinos, in *Indian Journal of Radio and Space Science*. Vol. 41. pp. 7–16.
- Smirnov, Y. G., Valovik, D. V., 2013. On the Problem of Electromagnetic Waves Propagating along a Nonlinear Inhomogeneous Cylindrical Waveguide, *ISRN Mathematical Physics*, Article ID 184325, 7 pages, Vol. 2013.
- Stål, O., 2007. Prospects for Lunar Satellite Detection of Radio Pulses from Ultrahigh Energy Neutrinos Interacting with the Moon, *Phys. Rev. Lett.*, 98(7):071103.
- ter Veen, S., Buitink, S., Falcke, H., et al., 2010. Limit on the ultrahigh-energy cosmic-ray flux with the Westerbork synthesis radio telescope , *Phys. Rev. D* 82, 103014.
- Weiler, T. J., 2003. Physics with Cosmic Neutrinos, PeV to ZeV, *Int. J. Mod. Phys. A*. Vol. 18. p. 4065.
- Williams, D., 2004. The Askaryan Effect and Detection of Extremely High Energy Neutrinos in the Lunar Regolith and Salt, Dissertation, University of California.
- Zarka, P., Bougeret, J.-L., Briand, C., et al., 2012. Planetary and Exoplanetary Low Frequency Radio Observations from the Moon, P&SS, in the special issue SPME, Issue 1. Vol. 74. pp. 156–166.
- Zas, E., Halzen, F., Stanev, T., 1992. Electromagnetic pulses from high-energy showers: Implications for neutrino detection, *Phys. Rev. D* 45, 362 .